# IRE1α regulates macrophage polarization, PD-L1 expression and tumor survival

By

Alyssa Batista[1]*, Jeffrey J. Rodvold[1*], Su Xian[2], Stephen Searles[1], Alyssa Lew[1], Takao Iwawaki[3], Gonzalo Almanza[1], T. Cameron Waller[2], Jonathan Lin[4], Kristen Jepsen[5], Hannah Carter[2], and Maurizio Zanetti[1]

[1] The Laboratory of Immunology
Department of Medicine and Moores Cancer Center
University of California, San Diego
9500 Gilman Drive
La Jolla, CA 92093-081

[2]Division of Medical Genetics; Department of Medicine,
And Bioinformatics and Systems Biology Program
University of California San Diego
La Jolla, CA 92093

[3]Laboratory for Cell Recovery Mechanisms
Brain Science Institute
RIKEN, 2-1 Hirosawa, Wako, Saitama 351-0198
Japan.

[4]Department of Pathology
Stanford University
300 Pasteur Drive
Palo Alto, CA 94305

[5]IGM Genomics Center
University of California, San Diego
9500 Gilman Drive
La Jolla, CA 92093-0612.

* These authors contributed equally

Corresponding author: Maurizio Zanetti

Ph: (858) 822-5412
FAX: (858) 822-5421
Email: mzanetti@ucsd.edu

## ABSTRACT

In the tumor microenvironment local immune dysregulation is driven in part by macrophages and dendritic cells that are polarized to a mixed proinflammatory/immune suppressive phenotype. The unfolded protein response (UPR) is emerging as the possible origin of these events. Here we report that the inositol-requiring enzyme 1 (IRE1α) branch of the UPR is directly involved in the polarization of macrophages *in vitro* and *in vivo,* including the upregulation of IL-6, IL-23, Arginase1, as well as surface expression of CD86 and PD-L1. Macrophages in which the IRE1α/Xbp1 axis is blocked pharmacologically or deleted genetically have significantly reduced polarization, and CD86 and PD-L1 expression, which was induced independent of IFNγ signaling suggesting a novel mechanism in PD-L1 regulation in macrophages. Mice with IRE1α- but not Xbp1-deficient macrophages showed greater survival than controls when implanted with B16.F10 melanoma cells. Remarkably, we found a significant association between the IRE1α gene signature and *CD274* gene expression in tumor-infiltrating macrophages in humans. RNASeq analysis showed that bone marrow derived macrophages with IRE1α deletion lose the integrity of the gene connectivity characteristic of regulated IRE1α-dependent decay (RIDD) and the ability to activate *CD274* gene expression. Thus, the IRE1α/Xbp1 axis drives the polarization of macrophages in the tumor microenvironment initiating a complex immune dysregulation leading to failure of local immune surveillance.

# INTRODUCTION

Myeloid cells in the tumor microenvironment (TME) are of central relevance to understand the dynamics of tumor progression [1]. They infiltrate tumors in varying numbers depending on tumor types and display phenotypic and functional diversity [2, 3]. Among them macrophages and dendritic cells -cells privileged with antigen presentation/T cell activation functions- often acquire a mixed pro-inflammatory/immune suppressive (IIS) phenotype, both in the mouse [4, 5] and in humans [6, 7]. Because this phenomenon is considered at the root of the dysregulation of local adaptive T cell immunity [8, 9], much emphasis has been placed on identifying common mechanisms driving the acquisition of tumor-promoting properties by macrophages and dendritic cells in the TME [5, 10-14].

The TME is home to environmental *noxae* such as hypoxia and nutrient deprivation [15]. In addition, about 20% of tumors have a viral origin [16] and most (90%) solid tumors carry chromosomal abnormalities [17]. These events, independently or collectively, can lead to a dysregulation of protein synthesis, folding, and secretion [18, 19], and the accumulation of misfolded proteins within the endoplasmic reticulum (ER), triggering a stress response termed the unfolded protein response (UPR) [20]. The UPR, an evolutionarily-conserved adaptive mechanism [21], is mediated by three initiator/sensor ER transmembrane molecules: inositol-requiring enzyme 1 (IRE1α), PKR-like ER kinase (PERK), and activating transcription factor 6 (ATF6). In the unstressed state these three sensors are maintained inactive through association with the 78-kDa glucose-regulated protein (GRP78) [22]. During ER stress, GRP78 disassociates from each of the three sensors to preferentially bind un/misfolded proteins, activating each sensor and their downstream signaling cascades, which aim to normalize protein folding and secretion. PERK, a kinase, phosphorylates the translation initiation factor 2 (eIF2α) that effectively inhibits translation of most mRNAs,

ultimately reducing ER client proteins. IRE1α, also a kinase, auto-phosphorylates and activates its RNase domain, resulting in the cleavage of the X-box binding protein 1 (XBP1) mRNA, yielding the production of the potent spliced XBP1 transcription factor isoform (XBP-1s), which drives the production of various ER chaperones to restore ER homeostasis. XBP-1s also binds to the promoter of several pro-inflammatory cytokine genes [23]. In addition, under ER stress or enforced autophosphorylation, IRE1α RNase domain can initiate an endonucleolytic decay of many ER-localized mRNAs, a phenomenon termed regulated IRE1α-dependent decay (RIDD) [24]. ATF6, a transcription factor, translocates to the Golgi where it is cleaved into its functional form, and acts in parallel with XBP-1s to restore ER homeostasis [25]. If ER stress persists despite these compensatory mechanisms, the transcription factor 4 (ATF4) downstream of eIF2α activates the transcription factor CCAAT-enhancer-binding protein homologous protein (CHOP) to initiate apoptosis [20].

Although the UPR serves essentially as a cell-autonomous process to restore proteostasis, it can also act in a cell-nonautonomous way through the release of soluble molecules, a phenomenon likely to occur when cancer cells undergo an acute or unresolvable UPR [26, 27]. Stress signals emanating from the ER of ER stressed cancer cells may thus result in the induction of ER stress in neighboring cells, including macrophages and dendritic cells [26, 28]. This sets in motion a broad range of adaptive responses creating a functional cooperation or community effect among cells in the TME [29-31]. Under controlled experimental conditions bone marrow-derived macrophages and dendritic cells (BMDM and BMDC) cultured in conditioned media of ER stressed cancer cells develop a de novo UPR and acquire a mixed IIS phenotype [26, 28] characterized by the transcriptional upregulation of the tumorigenic pro-inflammatory cytokines IL-6, TNFα, and IL-23 [32-34], and contextually of the immune-suppressive enzyme Arginase 1 (Arg1) [35]. Under these

conditions, cross-priming of naïve $CD8^+$ T cells by BMDC is greatly compromised [28]. In line with this observation, Cubillos-Ruiz reported that the incubation of BMDC in ovarian cancer conditioned media results in *Xbp1* splicing, and that the conditional knock-out of *Xbp1* in dendritic cells improves antigen presentation and significantly reduces tumor growth *in vivo* [36]. In line with these observation is a report showing that GRP78 in cancer cells regulates macrophage recruitment to mammary tumors through metabolites secreted from cancer epithelial cells [37]. Thus, UPR-driven cell-nonautonomous mechanisms play a hitherto unappreciated role in orchestrating immune cells in the TME and driving their dysregulation, so as setting the stage for failure of local immune surveillance.

We therefore decided to elucidate the mechanism(s) through which the UPR may ultimately affect immune cells and perturb the TME to promote tumor growth. We focused on macrophages as these cells represent the major population infiltrating most solid tumors in humans, conspicuously more abundant than dendritic cells and other cells of myeloid origin [38]. Relative to dendritic cells or myeloid derived suppressor cells (MDSCs) [39, 40] little is known about how the UPR affects macrophages during cancer development. Based on our earlier report that BMDM can be polarized to a mixed IIS phenotype via a UPR-mediated cell-nonautonomous mechanism [26] our initial goal was to verify whether this phenomenon could be recapitulated in tumor-infiltrating macrophages *in vivo* in immunocompetent mice, and what UPR pathway might contribute to their dysregulation. To this day, these questions have remained largely unanswered. Here we show that the UPR and the IRE1α/XBP1 axis are activated in macrophages during tumor growth, that the conditional knock-out of IRE1α in macrophages regulates the acquisition of a mixed IIS phenotype and is also sufficient to restrain tumor development *in vivo*. Importantly, we discovered that IRE1α signaling regulates PD-L1 expression in murine and in tumor-infiltrating macrophages in humans.

# RESULTS

## Tumor infiltrating CD11b$^+$ myeloid cells display the UPR/IIS signature *in vivo*

Previous *in vitro* studies indicated that BMDC and BMDM respond to a cell-nonautonomous UPR developing a complex phenotype characterized by a UPR activation and a mixed pro-inflammatory/immune suppressive (IIS) phenotype [26, 28]. Here as an initial step we interrogated tumor-infiltrating myeloid cells (CD11b$^+$) to document these characteristics during tumor growth *in vivo*. To this end, we implanted B16.F10 murine melanoma cells into C57BL/6 mice that carry the *Xbp1-Venus* fusion transgene under the control of the CMV-β actin promoter, known as the ER stress-activated indicator (ERAI) [41], which reports IRE1α mediated *XBP1* splicing through the expression of the fluorescent Venus protein. First, we interrogated the relative abundance of CD11b$^+$ cell infiltrate into tumors three weeks after implantation of B16.F10 tumor cells and found that 2-5 % of the bulk tumor consisted of CD11b$^+$ myeloid cells (Fig. S1). Of these ~50% expressed the F4/80 surface marker specific of macrophages. We then compared the expression of the *Venus* protein in tumor-infiltrating CD11b$^+$ cells to those in the spleen and bone marrow, both from tumor-distal and tumor-proximal femurs (Fig 1A). The *Venus* protein signal was significantly higher in tumor-infiltrating CD11b$^+$ cells relative to those in control tissues, suggesting a concurrent UPR signaling with *XBP1* splicing in the TME only.

Having established that *XBP1* splicing occurs in tumor-infiltrating CD11b$^+$ cells, we sought to detect other features of the IIS phenotype. To this end, we implanted B16.F10 cells in wild-type C57BL/6 mice and isolated by positive selection CD11b$^+$ cells from tumor, spleen and bone marrow 22 days post-implantation. Phenotypically, the isolated cells were CD11b$^+$ and Gr1$^-$ and showed the transcriptional upregulation of three key UPR genes: *Grp78*, a downstream target of the ATF6 pathway, spliced *Xbp1* (*Xbp1-s*) a downstream

product of the IRE1α pathway, and *Chop*, a downstream product of the PERK pathway (Fig. 1B). A transcriptional upregulation of all three genes suggested the activation of a classical UPR. Contextually, $CD11b^+$ cells also showed the transcriptional upregulation of *Il23p19,* a key pro-inflammatory cytokine gene, and Arginase-1 (*Arg1*), an immune suppressive enzyme (Fig. 1C).

To see if the UPR/IIS signature also hallmarks $CD11b^+$ cells during spontaneous tumor growth, we interrogated mice with mutations in the adenomatous polyposis coli (*Apc*) gene ("Apc mice"), which develop small intestinal adenomas by 30 days of age [42]. We pooled $CD11b^+$ cell infiltrates from adenomas from multiple Apc mice and probed the expression of UPR genes, *Il-23p19* and *Arg1* relative to $CD11b^+$ cells isolated from either the bone marrow or the spleen as controls. $CD11b^+$ cells from APC adenomas had increased expression of UPR genes, *Il-23p19* and *Arg1* (Fig. 1D,E). Collectively, these data suggest that $CD11b^+$ cells infiltrating the TME undergo ER stress and are polarized to the IIS phenotype.

## IRE1α dependent cell-nonautonomous polarization of macrophages

Environmental conditions shown to have tumor promoting effects have been linked to both IRE1α and PERK, making it necessary to determine which of the two was responsible for the acquisition of the IIS phenotype in our model system. To probe the role of IRE1α, we used the small molecule 4μ8C, an inhibitor specific for the RNAse domain. This small molecule forms an unusually unstable Schiff base at lysine 907 (K907) and inhibits both XBP1 splicing and regulated IRE1α-dependent decay (RIDD), but not IRE1α kinase activity. To confirm that 4μ8c (30 μM ) was effective we measured *Xbp-1* splicing in C57Bl/6 BMDM and B16.F10 cells treated with the conditioned medium (CM) of ER stressed cancer cells (transmissible ER stress conditioned medium or "TERS CM") (Fig. S2). Compared to

uninhibited conditions, 4μ8C did not significantly affect the transcriptional of UPR genes (*Grp78* and *Chop*, Fig. 2A). However, it significantly inhibited the transcriptional activation of *Il-6* and *Il-23p19* (Fig. 2B) and trended towards inhibiting *Arg1* (p=0.127) (Fig. 2C). Previously, we showed that TERS CM promotes the expression of CD86 and PD-L1 in BMDC [28]. Herein, we determined that ERAI BMDM treated with TERS CM also upregulate CD86 and PD-L, and that such an upregulation that is markedly inhibited by 4μ8C (Fig. 2D).

The involvement of the PERK pathway on the acquisition of the IIS phenotype by BMDM was assessed using the small molecule GSK2656157, a preferential PERK inhibitor [43]. GSK2656157 efficiently inhibited PERK phosphorylation (Fig S3A) but had no effect on the upregulation of *Grp78, Il-6* and *Arg1* induced in BMDM cultures by TERS CM (Fig. S3B). Congruently, PERK inhibition had little to no effect on the surface expression of CD86 and PD-L1 (Fig S3C). Collectively, these results suggest that BMDM polarization to the IIS phenotype is IRE1α dependent. ~~.~~

The role of IRE1α during macrophage activation by stimuli not obviously related to the UPR was tested in experiments in which BMDM were activated by LPS, a canonical activator of macrophages, or two metabolites shown to be relevant to the function of myeloid cells in the tumor microenvironment: lactic acid [10] and 4-hydroxynonenal (4-HNE), a products of lipid peroxidation [36]. While none of these molecules induced the transcriptional activation of *Gr78,* LPS consistently and readily induced *Il23p19* and *Il6* independent of IRE1α. Lactic acid induced *Arg1* only, and 4HNE had no effect on any of the target genes studied. Interestingly, 4μ8C reduced the induction of *Arg1* by both LPS and lactic acid, suggesting that the IRE1α may regulate the expression of this immune suppressive molecule outside the context of the UPR (Fig. S4).

## Loss of IRE1α–Xbp1 in macrophages attenuates the IIS phenotype, PD-L1 expression and tumor growth *in vivo*

Earlier reports showed that XBP1 is required for the development and survival of bone marrow derived DC [44], and that the deletion of XBP1 in lymphoid DC [40, 45] or in tumor-associated DC [36] improves antigen cross-priming and reduces tumor (ovarian) growth in the mouse. The role of the IRE1α/XBP1 axis in macrophage activation in the context of tumorigenesis has not been previously explored. Chemical inhibition of IRE1α endonuclease activity clearly implicated the IRE1α pathway in macrophage polarization to the IIS phenotype. However, since 4μ8C inhibits both *Xbp1* splicing and RIDD activity [46], we used a genetic approach to distinguish mechanistically among the two IRE1α functions in the acquisition of the IIS phenotype. To this end, we developed mice with *Ern1* (the gene coding for IRE1α) or *Xbp1* conditional knockout (CKO) in macrophages by breeding mice floxed (*fl/fl)* for *Ern1* [41] or *Xbp1* [47] with LysM-Cre mice (B6.129P2-Lys2tm1(cre)Ifo/J [48]. The genotype of CKO mice is shown in Fig. S5. Western blot analysis of *Ern1* CKO BMDM confirmed the absence of IRE1α (Fig. 3A) as well as the absence of the spliced form of *Xbp1* following treatment with the SERCA (sarco/endoplasmic reticulum $Ca^{2+}$-ATPase) inhibitor thapsigargin (Fig. 3B). Under similar experimental conditions, *Xbp1* CKO BMDM showed an intact IRE1α expression under basal conditions (Fig. 3A) but the absence of the spliced form of *Xbp1* after thapsigargin treatment (Fig. 3C). Thus, the LysM-Cre CKO system was effective at specifically deleting IRE1α and Xbp1 in activated BMDM.

First we compared the transcriptional response of *Ern1* and *Xbp1* CKO vs wild type BMDM when treated with TERS CM. We found that *Grp78* and *Chop* were unaffected in *Ern1* CKO BMDM, but *Il6*, *Il-23p19* and *Arg1* were markedly and significantly reduced in CKO relative to *fl/fl* control BMDM (Fig. 3D, upper panels). Likewise, in *Xbp1* CKO

BMDM, the induction of *Grp78* and *Chop* was unaffected, but the activation of *Il6* and *Il23p19* was significantly reduced compared to *fl/fl* control BMDM. The activation of *Arg1* trended lower in *Xbp1* CKO compared to *fl/fl* control BMDM ($p = 0.0571$). (Fig. 3D, lower panels). These results confirm that the IRE1α-XBP1 axis mediates the IIS phenotype.

We then evaluated the effect of TERS CM on the expression of CD86 and PD-L1 in BMDM populations. *In vitro* treatment of *Ern1* or *Xbp1* CKO BMDM with TERS CM yielded a significant reduction of both surface proteins compared to wild type BMDM (Fig. 3E). Thus, the conditional deletion of the IRE1α/XBP1 axis in macrophages produced effects consistent with the pharmacological inhibition by 4μ8C. This suggests that the IRE1α-XBP1 axis is central to both macrophage activation (CD86 upregulation) and the acquisition of PD-L1, a marker of immune disfunction. We ruled out the possibility that PD-L1 expression was the result of canonical IFN-γ signaling since (a) we did not detect IFN-γ in TERS CM (Fig. S6A), (b) a blocking antibody to human IFN-γ had no effect on *Cd274* gene expression in BMDM treated with TERS CM (Fig. S6B), and (c) RNASeq data showed no induction of the *Ifng* gene in either *Ern1* CKO or *fl/fl* control BMDM treated with TERS CM (Fig. S6C).

To ascertain the physiological relevance of these findings, we next assessed the survival of *Ern1* and *Xbp1* CKO mice implanted with B16.F10 melanoma cells. We reasoned that survival would constitute an optimal initial read-out for the complex interactions between cancer cells and immune cells in the TME with focus on the IRE1α-XBP1 axis in myeloid cells. Survival in *Ern1* CKO mice was significantly greater ($p=0.03$) than in control *Ern1 fl/fl* mice (Fig. 4A). By contrast, *Xbp1* CKO mice survived longer than control *Xbp1 fl/fl* mice but the difference was non-significant (Fig. 4A). Based on survival data we isolated F4/80 tumor-infiltrating macrophages of tumor-bearing *Ern1* CKO mice to assess the UPR/IIS and *Cd274* gene expression status. *Xbp1s*, *Il-23p19*, *Arg1 and Cd274 genes* were all markedly

reduced in *Ern1* CKO macrophages compared to their *Ern1 fl/fl* counterpart (Fig. 4B). Together, these results point to macrophage IRE1α as a key negative regulator of TME immunodynamics and tumor growth *in vivo*.

**Loss of RIDD regulation in *Ern1* CKO macrophages**

Because the IRE1α-XBP1 axis also regulates PD-L1 expression and both *Ern1* and *Xbp1* CKO BMDM showed significantly-reduced surface PD-L1 protein expression compared to *fl/fl* BMDM (Fig. 3E), we decided to distinguish the relative contribution of *Xbp1* splicing and RIDD to this phenomenon. To this end, we performed RT-qPCR on *Ern1*- and *Xbp1* CKO BMDM treated or not with TERS CM relative to *fl/fl* controls. We found that *Cd274* gene transcription was markedly and significantly lower in *Ern1* CKO BMDM relative to *fl/fl* controls (Fig. 5A). By contrast, *Xbp1* CKO BMDM and *fl/fl* BMDM had comparable *Cd274* gene transcription values (Fig. 5A). Based on this result and on PD-L1 surface expression (Fig. 3E), we tentatively conclude that XBP1-mediated regulation of PD-L1 occurs at the post-translation level, whereas IRE1α-mediated regulation is a transcriptional event. This conclusion favors the view that IRE1α-mediated PD-L1 regulation may occur via RIDD, justifying an in-depth analysis of RIDD activity in *Ern1* CKO BMDM.

We performed RNASeq analysis of *fl/fl* and *Ern1* CKO BMDM untreated or treated with TERS CM. Three independently-derived BMDM populations per group were analyzed. The genotype of each mouse used in this experiment is shown in Fig. S5. Upon TERS CM treatment *Ern1* expression in *Ern1* CKO macrophages was 1.79-fold over that of untreated cells compared to 3.26 fold in *fl/fl* macrophages (Fig. 5B). We found that consistent with the flow cytometry data, *Cd274* (PD-L1) expression was markedly increased in macrophages (44.45-fold) but only moderately increased in *Ern1* CKO macrophages (4.11-fold, Fig 5C). Thus, both genetic and chemical inhibition of IRE1α signaling yielded concordant results.

Next, we performed a comprehensive analysis of RIDD activity using a set of 33 putative RIDD target genes previously defined [49]. We found that only half (sixteen) of these genes behaved as *bona fide* RIDD targets in TERS CM-treated BMDM (i.e., decreased expression after TERS CM treatment in *fl/fl* macrophages) (Fig. 5D, upper panel). We found that in *Ern1* CKO macrophages, there was a clear loss of a "RIDD signature" compared to *fl/fl* macrophages, both basally and after TERS CM treatment (Fig. 5D, lower panel). When considered together through an analysis of the mean z-score for the 16 genes, it became apparent that TERS CM induction of RIDD activity was much more effective in *fl/fl* than in *Ern1* CKO macrophages (Fig. 5E). Collectively, these results show that macrophages lacking *Ern1* lose RIDD regulation, suggesting that RIDD may be implicated in the regulation of PD-L1 expression.

In the same analysis we found that *Tabpb* (tapasin), a chaperone molecule involved in the stabilization of high affinity peptide/MHC-I complexes in the endoplasmic reticulum [50], did not behave as RIDD. In fact, *fl/fl* macrophages treated with TERS CM showed *increased* not diminished expression at variance with previous reports on lymphoid ($CD8\alpha^+$) dendritic cells [40, 45]. The expression of *Bloc1s1* (a canonical RIDD target) was reduced, confirming that TERS CM induces RIDD (Fig. S7A). RT-qPCR analysis of *Tapbp* in *Xbp1 fl/fl* macrophages showed similar results (Fig. S7B). Perhaps, *Tapbp* is regulated by RIDD differently in $CD8\alpha^+$ dendritic cells and in BMDM.

**A link between IRE1α and PD-L1 expression in human tumor-infiltrating macrophages**

The data reported herein suggest that *Cd274* gene expression in murine macrophages is positively regulated by IRE1α. Recently, Xu et al. [51] reported that PD-L1 protein expression in murine $MYC^{tg}$:$KRAS^{G12D}$ tumor cells is decreased by a small molecule that enables the cell to resume translation while the eIF2α downstream from PERK remains

phosphorylated. Therefore, we decided to study the relationship between *CD274* (PD-L1) gene expression and the two major UPR pathways, IRE1α and PERK, across multiple human cancers. We began by interrogating the relative contribution of *ERN1* (IRE1α) and *EIF2AK3* (PERK) to *CD274* gene expression. In this analysis, we queried The Cancer Genome Atlas (TCGA) collection of RNA-sequencing expression data for bulk samples from thirty-one tumor types. Across these data, we observed that *ERN1* correlates strongly with *EIF2AK3* (Pearson correlation coefficient = 0.55; $p < 1e\text{-}200$) (Fig. S8A), and that both *ERN1* ($p \leq 1.46e\text{-}51$) and *EIF2AK3* ($p \leq 1.62e\text{-}44$) correlate positively with *CD274*, suggesting that the UPR plays a role in *CD274* gene expression. These correlations prompted us to further interrogate the relationship between *CD274*, *ERN1* and *EIF2AK3,* with respect to levels of infiltrating macrophages in bulk tumor samples approximated by a macrophage score derived from the geometric mean of three genes expressed by macrophages (*CD11b*, *CD68*, and *CD163)*. We found a positive correlation between *ERN1* and *CD274* within the high macrophage infiltration group ( > 70th percentile) (Spearman correlation coefficient 0.18; $p < 1.3e\text{-}21$) (Fig. S8B). By contrast, the low macrophage infiltration group (< 30$^{th}$ percentile) had a much weaker correlation (Spearman correlation coefficient 0.06; $p < 0.001$) (Fig. S8B). On the other hand, *EIF2AK3* and *CD274* within the high macrophage infiltration group ( > 70th percentile) had a lower correlation (Spearman correlation coefficient 0.09; $p < 1.9e\text{-}7$) than in the corresponding *Ern1* group (Fig. S8C). Finally, *EIF2AK3* and *CD274* within the low macrophage infiltration group (< 30th percentile) had a surprisingly higher correlation (Spearman correlation coefficient 0.15; $p < 8.32\text{-}15$) than in the respective high macrophage infiltration group (Fig. S8C). Collectively, this analysis suggests that when macrophage infiltration is high, *Ern1* is a better predictor of *CD274* gene expression than *EIF2AK3*.

We also integrated the macrophage score with *ERN1* and *EIF2AK3* to predict *CD274* expression in an ordinary least squares (OLS) linear regression model, including the tumor

type as a covariate (Table 1). We found that this model assigns significant, positive coefficients for the interaction terms of macrophages with *ERN1* (*ERN1**Macrophages, beta coefficient = 0.0012, $p < 0.023$) but not *EIF2AK3* (*EIF2AK3**Macrophages, beta coefficient = 0.0007, $p < 0.155$), suggesting that *ERN1* but not *EIF2AK3* is predictive of *CD274* gene expression within tumor-infiltrating macrophages in individual tumor types (Table 1). To validate these results we analyzed RNA-Seq data generated from macrophages isolated from thirteen patients with either endometrial or breast cancer [52]. We found a strong Pearson correlation coefficient between *ERN1* and *EIF2AK3* in these data (correlation coefficient 0.738; $p < 0.003$), suggesting UPR activation. Since IRE1α activity is a multistep and complex process [53] and may not be completely captured by *ERN1* expression levels, we derived a systemic representation of pathway activity controlled by IRE1α and by comparison PERK. We collected sets of downstream genes in the IRE1α and PERK pathways [54], and derived aggregate scores for each pathway from the mean expression signal of all detectable genes after z-score transformation. Since the transformed pathway scores could potentially amplify noise from genes with low expression, we applied filters to include only genes in each pathway with levels beyond a specific threshold (Fig. S9). We varied this filter threshold from zero to one thousand raw counts and then included the pathway activity scores in multiple OLS linear models to predict *CD274* across tumor-infiltrating macrophage samples (Fig. 6A). We found that a filter threshold of 100 counts effectively reduced noise while preserving signal from 84% of detectable genes in both the IRE1α and PERK pathways. In this model, the IRE1α score predicted *CD274* expression with a significant positive beta coefficient (beta coefficient = 21.043, p-value = 0.040), while the PERK score was non-significant (beta coefficient = 36.842, p-value = 0.103). This pattern of significant IRE1α coefficient and nonsignificant PERK coefficient was consistent across all filter thresholds (Fig. 6B). Comparing models wherein *CD274* expression was

357 explained by IRE1α activity alone or by both IRE1α and PERK activity using the Aikake
358 information criterion analysis shows that a model containing both is as 0.54 times as probable
359 as the IRE1α alone to minimize the information loss (ΔAIC = 1.23). Taken together, these
360 analyses suggest that the activation of *CD274* gene expression in tumor-infiltrating
361 macrophages depends primarily on the IRE1α pathway.

362

## 363 DISCUSSION

364 Here we analyzed the effect of the UPR on gene expression regulation in macrophages as a
365 potential mechanism driving immune dysregulation in the tumor microenvironment. Tumor-
366 infiltrating $CD11b^{+}$ myeloid cells in B16.F10 tumors and in spontaneously-arising colonic
367 adenomas in Apc mice have an active UPR and display a mixed pro-inflammatory/immune
368 suppressive phenotype. Using both a pharmacologic and genetic approach we show that the
369 IRE1α/XBP1 axis plays a central role in macrophage activation and polarization to a mixed
370 phenotype, including the upregulation of PD-L1. In agreement with the mouse data we found
371 that in human tumor-infiltrating macrophages *CD274* (PD-L1) gene transcription correlates
372 significantly with the IRE1α gene signature. B16.F10 tumor-bearing mice with conditional
373 *Ern1*- but not *Xbp1* KO macrophages had significantly greater survival than their *fl/fl*
374 controls. Collectively, these results show that IRE1α signaling drives macrophage
375 dysregulation impacting negatively the immunobiology of the tumor microenvironment and
376 ultimately the host's ability to control tumor growth.

377 Virtually all adult solid tumors (carcinomas most notably) contain infiltrates of
378 diverse leukocyte subsets, including macrophages, dendritic cells, and lymphocytes [2].
379 CIBERSORT and immunohistochemical tools have previously shown that macrophages

represent the largest fraction among infiltrating leukocytes and their density correlates directly with poor survival [38, 55]. In the mouse, tumor-infiltrating CD11b$^+$ myeloid cells produce pro-inflammatory/pro-tumorigenic cytokines (IL-6, IL-23, TNFα) [32-34], but oddly, also anti-inflammatory cytokines (IL-10, TGFβ) and molecules with immune suppressive function (Arginase1, perioxinitrite and indoleamine 2-3 dioxygenase) [8]. In humans, monocytes/macrophages with a "mixed" pro-inflammatory/suppressive phenotype have been reported in patients with renal cell carcinoma [6] and breast cancer [7]. Thus, a dysregulation-prone TME harbors CD11b$^+$ myeloid cells with a split pro-inflammatory/immune suppressive phenotype that may be the result of hijacking by tumors for their own benefit [56]. Indeed, we previously proposed that tumor-derived UPR-driven factors determine the IIS phenotype in myeloid cells [57], contributing to progressive immune dysregulation and failure of immune surveillance.

Here, we analyzed two murine tumor models to demonstrate that tumor-infiltrating CD11b$^+$ cells display features of UPR activation and a mixed IIS phenotype. The results clearly show that the UPR is associated with myeloid cell polarization *in vivo*, but do not allow a distinction between a cell-autonomous and a cell non-autonomous mechanism. However, since common triggers of inflammation such as LPS, or TME metabolites such as 4HNE and lactic acid [10, 36], did not induce a UPR/IIS phenotype, we favor the possibility that these changes in myeloid cells result from a cell non-autonomous mechanism of intercellular communication consistent with findings on BMDM and BMDC analyzed under controlled *in vitro* conditions [26, 28]. This appears to be a general mechanism since we recently showed that cell-nonautonomous intercellular communication among cancer cells induces an adaptive UPR imparting receiver cells with enhanced cellular fitness and resistance to various stressors [27].

A pharmacological approach using a small molecule (4μ8c) that inhibits IRE1α significantly reduced the transcription of *Il-6* and *Il-23p19* induced by TERS CM demonstrating a direct involvement of the IRE1α/XBP1 axis in driving pro-inflammation during an adaptive UPR. This is consistent with previous reports showing that XBP1 is recruited to the *Il6* and *Il23* promoters [23] and that *Il23* transcription is IRE1α-dependent [58]. Interestingly, 4μ8C did not reduce the transcription of these cytokines in the absence of a UPR, implying that IRE1α selectively regulates pro-inflammation within the boundaries of the UPR. Our findings on macrophage polarization via cell-nonautonomous means are consistent with reports showing that IRE1α drives M1 to M2 polarization of macrophages within white adipose tissue [59] and their inflammatory response to saturated fatty acids [60]. Importantly, 4μ8C also inhibited the TERS CM-induced upregulation of *Arg1,* and that of pro-angiogenic vascular endothelial growth factor (VEGF) (Fig. S10). Since IL-6 and IL-23 are known to bias T cell differentiation towards inflammatory (Th17) or regulatory T cells [61-65], and Arg1 potently suppresses the clonal expansion of T cells activated by antigen [28, 35], it follows that signaling through the IRE1α/XBP1 axis is of paramount importance to the economy of the TME and may be at the origin of a loss of local immune surveillance.

*Ern1* or *Xbp1* CKO macrophages enabled us to distinguish different roles within the IRE1α/XBP1 axis relative to immune dysregulation and tumor growth. *In vitro*, both *Ern1*- and *Xbp1*-CKO BMDM had decreased activation (CD86 and PD-L1 surface expression) and an attenuated IIS phenotype compared to control *fl/fl* macrophages when cultured in TERS CM, consistent with the effects of 4μ8C. However, only IRE1α deficiency significantly increased survival of mice implanted with B16.F10 melanoma cells, a result possibly reflected by an attenuation of the UPR/IIS signature and PD-L1 in tumor-infiltrating macrophages. Cubillos-Ruiz [36] also observed that IRE1α deficiency in DCs yielded

428 greater survival than XBP1 deficiency in a model of ovarian cancer. By inference, we
429 showed that B16.F10 tumor cells admixed with bone marrow-derived DCs with a UPR/IIS
430 phenotype form faster-growing and larger tumors that had a marked reduction in tumor-
431 infiltrating $CD8^+$ T cells [28].

432 Chemical and genetic inhibition both showed that IRE1α regulates the surface
433 expression of PD-L1 triggered in an IFNγ-independent manner through an adaptive UPR.
434 PD-L1 activation is considered to occur mainly in response to IFNγ, albeit other mechanisms
435 can contribute to its activation both at the transcriptional and post-translational levels [66].
436 The inhibition of cell surface PD-L1 upregulation during the UPR by either pharmacological
437 or genetic means indicates that the IRE1α/XBP1 axis functions as a gatekeeper of PD-L1
438 expression in macrophages independently of IFNγ produced locally by T cells. By comparing
439 gene expression in *Ern1*- and *Xbp1*-CKO macrophages it became apparent that *Ern1* but not
440 *Xbp1* regulates a UPR-mediated PD-L1 gene expression.

441 Mouse studies showed that the sensitivity to PD-L1 blockade depends on PD-L1
442 expression in myeloid cells (macrophages and dendritic cells) and not on tumor cells [67,
443 68]. Remarkably, a recent report showed that ISRIB, a small molecule that reverses the
444 effects of eIF2α phosphorylation downstream of PERK, reduces the abundance of the PD-L1
445 protein in murine $MYC^{Tg};KRAS^{G12D}$ liver cancer cells [51]. Whereas both reports agree on
446 the role of the UPR in regulating PD-L1 expression, the discrepancy between the two studies
447 creates an interesting conundrum as to why PD-L1 might be under the control of two
448 different arms of the UPR in myeloid and tumor cells, respectively. Significantly, our
449 analysis of tumor-infiltrating macrophages isolated from human endometrial and breast
450 cancers indicates that the IRE1α gene signature is a better predictor of *CD274* (PD-L1)
451 transcription than the PERK gene signature, confirming the conclusion reached in mouse

macrophages, pointing to IRE1α as an important IFNγ-independent regulator of *CD274* in macrophages. Since PD-L1 serves as the ligand for PD-1$^+$ T cells with exhausted [69] or regulatory phenotype [70], a plausible conclusion from the present study is that IRE1α inhibition in tumor-infiltrating myeloid cells could be used therapeutically to ameliorate the effects of immune dysregulation in the TME, including the downregulation of PD-L1, ultimately rescuing a failing immune surveillance and restoring immune competence locally.

A RIDD analysis in *Ern1* deficient macrophages showed a dramatic loss of the integrity and connectivity of RIDD genes compared to control (*Ern1 fl/fl)* macrophages. This provides initial mechanistic evidence that RIDD may be involved in shaping the immune landscape in the TME, including PD-L1 expression. A possibility is that upon IRE1α activation, RIDD degrades not only mRNAs but miRNAs as well, among which is miR-34a [71, 72], a miRNA also shown to target *CD274* (PD-L1) mRNA by directly binding to its *3*'-UTR [73, 74]. The loss of RIDD integrity shown here suggests that RIDD / miR-34a could represent the link between IRE1α and *CD247* gene expression. Future studies will need to address the role of RIDD in PD-L1-driven immune dysregulation in the TME.

In conclusion, we provide evidence in support of UPR-driven mechanisms as a source of immune dysregulation in the tumor microenvironment. We have identified the IRE1α/XBP1 axis as a critical signaling pathway in macrophage polarization to a mixed pro-inflammatory/immune suppressive phenotype, PD-L1 expression and tumor growth. Cell-nonautonomous IRE1α-dependent signaling has been proposed as a regulator of immune activation [75] and stress resistance and longevity in *C. elegans* [76], suggesting that the IRE1α/XBP1 axis may be central to intercellular communication during cellular stress. Here we further validate the view that UPR signals in the TME directly affect tumor-infiltrating

476 macrophages promoting a complex immune dysregulation and defective tumor control *in*
477 *vivo*. The fact that the IRE1α/XBP1 axis also regulate PD-L1 expression point to the UPR as
478 a general mechanism for immune dysregulation at the tumor and immune cells interface
479 with myeloid cells ultimately impairing the function of tumor specific T cells [28, 36] with
480 loss of local immune surveillance.

481

# MATERIALS AND METHODS

## Cell lines and cell culture

Human cells lines colon carcinoma DLD1 and prostate PC3 and murine cell lines prostate TC1 and melanoma B16.F10 cancer cells were grown in RPMI or DMEM (Corning) supplemented with 10% FBS (HyClone) and 1% penicillin/streptomycin/L- glutamine, NEAA, sodium pyruvate, HEPES. All cells were maintained at 37°C incubation with 5% $O_2$. All cell lines were mycoplasma free as determined PCR assay (Southern Biotech).

## Mice

APC mice were provided as a kind gift from Dr. Eyal Raz (UCSD). LysM. B6.129P2-Lyz2 $^{tm1(cre)Ifo}$/J (LysM-Cre) mice were kindly provided by Dr. Richard Gallo (UCSD). ERN1$^{fl/fl}$ and XBP1$^{fl/fl}$ mice were kindly provided by Dr. Jonathan Lin (UCSD) who originally obtained them from Drs. Laurie Glimcher (Dana Farber, Harvard University) and Takao Iwawaki (RIKEN, Japan). All mice were housed in the UCSD vivarium according to approved protocols and animal welfare standards. Genotype of CKO mice were confirmed by PCR on tissue obtained by ear punch and digested according to a standard protocol.

## TERS Conditioned Medium (CM) Generation

DLD1 cells were induced to undergo ER stress through treatment of 300 nM thapsigargin (Tg) (Enzo Life Sciences) for 2 hours. Control cells were similarly treated with an equal volume of vehicle (0.02% ethanol). Cells were washed twice with Dulbecco's PBS (Corning), and then incubated in fresh, standard growth medium for 16 hrs. Conditioned medium was then harvested, centrifuged for 10 min at 2,000 RPM, filtered through a 0.22-µm filter (Millipore), and treated to cells or stored at -80°C until use. For TERS priming, conditioned media was generated from homologous cell type unless otherwise specified. To measure

IFNγ in TERS CM, QBeads (Intellicyt, Ann Arbor, MI) were used following manufacturer's instructions. IFNγ was quantified on the iQue Screener PLUS (Intellicyt) using a standard cursive and manufacturer-provided template for analysis.

**BMDM and BMDC generation in culture**

Bone marrow derived cells were procured by isolating the femur and tibia of specified host and flushing out the bone marrow using cold, unsupplemented RPMI growth media (Corning) using a 27 gauge needle and syringe. Hemolysis was performed using ACK Lysis buffer (Bio Whittaker). For macrophage differentiation, bone marrow cells were incubated one week in standard growth medium supplemented with 30% L929 conditioned medium (LCM) or m-CSF (origin) at concentration.

**ERAI activity assay**

Cancer cell line reporter cells were transduced with the ERAI construct, originally described (234). Briefly, the pCAX-F-XBP1ΔDBD-venus (a kind gift from Dr. Iwawaki, Gunma University) underwent PCR using following primers: F: ctaccggactcagatctcgagccaccATGGACTACAAGGACGACG, R: gaattatctagagtcgcggccgcTTACTTGTACAGCTCGTCC. PCR fragments were cloned into pLVX-puro (Clontech) lentivirus vector with Gibson Assembly Mixture (NEB) according to manufacturer's instruction. Stbl3 competent cells were transformed to produce the plasmid insert, whose presence was confirmed by sequencing. For production of lentivirus, 293FT (Invitrogen) cells were seeded in 10 cm dish and transfected with a plasmid mixture of ERAI plasmid and psPAX2 and pMD2G viral packaging plasmids. The supernatant of virus–producing transfected cells was collected every 24 hrs for three days post transfection. Viral supernatant was concentrated by 10% PEG-8000 and pelleted with 2000 x g for 40 min at 4C and re-suspended PBS. Target cancer cells were transduced with lentivirus by adding

529 supplementing with polybrene (8 μg/mL) to virus containing solution and loaded onto
530 B16.F10 cancer cell line. Lines were transduced for 48 hours. Following, cells were washed
531 twice with PBS and positively selected for using puromycin (2 μg/mL) for two weeks. In
532 some instances, positively transduced cells were then stimulated for Venus expression and
533 were sorted by FACS (BD) to isolate high expressing clones. Lines were maintained under
534 puromycin.

535 **Flow cytometry**

536 Single cell suspensions of myeloid cells were separated and stained for CD80 (B7- 1) (BD
537 Biosciences), PD-L1 (CD274) (BD Biosciences), and CD86 (BD Biosciences). Viable cells
538 were determined by 7AAD exclusion and data were acquired using a FACScalibur flow
539 cytometer (BD). Flow results were analyzed using CellQuest Pro (BD) and Flow JO (Tree
540 Star) software.

541 **RT-qPCR**

542 mRNA was harvested from cells using Nucleopsin II Kit (Machery-Nagel) or enzymatically
543 using the Zygem RNAgem Tissue PLUS kit (Microgembio, New Zealand). Concentration
544 and purity of RNA was quantified the NanoDrop (ND-1000) spectrophotometer (Thermo
545 Scientific) and analyzed with NanoDrop Software v3.8.0. RNA was normalized between
546 conditions and cDNA generated using the High Capacity cDNA Synthesis kit (Life
547 Technologies). RT-qPCR was performed on ABI 7300 Real-Time PCR system using
548 TaqMan reagents for 50 cycles using universal cycling conditions. Cycling conditions
549 followed manufacturer's specifications (KAPA Biosystems). Target gene expression was
550 normalized to *β-actin* and relative expression determined by using the –ΔΔCt relative
551 quantification method. Primers for qRT-PCR were purchased from Life Technologies: Arg1,
552 (Mm00475988_m1), Cd274 (Mm03048248_m1), Chop (Mm00492097_m1), Grp78

(Mm00517691_m1), Il6 (Mm99999064_m1), Il23-p19 (Mm00518984_m1), and Tapbp (Mm00493417_m1).

**Western Blot Analysis**

After treatment, cells were washed with ice cold PBS and suspended in the RIPA Lysis Buffer system: 1X RIPA buffer and cocktail of protease inhibitors (Santa Cruz Biotechnology). Cell lysates were centrifuged at 16,000g for 15 min and the supernatants were extracted. Protein concentration was determined using Pierce BCA Protein Assay Kit (Thermo Scientific). Samples were heat denatured and equal concentrations of protein were electrophoresed on 4-20% Mini-PROTEAN TGX Precast Gels (Bio-Rad) and transferred onto 0.2 μm PVDF membrane in Tris-Glycine transfer buffer containing 20 % methanol. The membranes were blocked with 5% non-fat milk in TBS containing 0.1 % Tween-20 (TBS-T) for 1 h at room temperature, and subsequently incubated with diluted primary antibodies overnight at 4 ℃. Membranes were washed for 5 min at room temperature 3 times by TBS-T, incubated with secondary antibody conjugated with horse radish peroxidase (HRP) in 5 % non-fat milk for 1 h at room temperature, and washed for 5 min at room temperature 3 times by TBS-T. Immuno-reactivity was detected by chemi-luminescence reaction using Pierce ECL Blotting Substrate (Thermo Scientific). Primary antibodies used were: rabbit monoclonal antibody to IRE1α (clone 14C10) (Cell Signaling Technology), rabbit polyclonal antibody to XBP-1s (#83418) (Cell Signaling Technology), goat polyclonal antibody to GAPDH (A-14) (Santa Cruz Biotechnology). Bound primary antibodies were revealed by the following secondary antibodies: HRP-conjugated goat antibody to rabbit IgG (Cell Signaling Technology), and HRP-conjugated donkey antibody to goat IgG (sc2020) (Santa Cruz Biotechnology).

**Tumor studies**

For orthotropic tumor implantation model, B16.F10 cancer cells (n=4) were detached from plastic, washed twice with cold PBS, and resuspended at a concentration of 3e5cells/ml in PSB. Host C57BL/6 or transgenic ERAI mice (a kind gift from Dr. T. Iwawaki (Gunma University)) were subcutaneously injected with 100 µl (3e4 cells) of cell suspension into the right hind flank. After approximately 22 days, mice bearing tumors greater than 1 cm were sacrificed. For tumor growth studies, B16.F10 were subcutaneously injected in C57BL/6 (WT) or TLR4 KO mice (a kind gift from Dr. M. Corr (UCSD)). Tumor establishment was first determined by palpation and size was then measured in two dimensions using calipers. When tumors reached > 20 mm in any one dimension or after 30 days post implantation, whichever came first, mice were sacrificed. Tumor volume was calculated using the ellipsoid volume formula, $V = 1/2\ (H \times W^2)$. All mice were sacrificed when any tumor reached 20 mm in any one dimension, per UCSD animal welfare standards, or after 30 days post implantation. Tumor volume was calculated using the ellipsoid formula: $V = ½\ (H \times W^2)$.

**Isolation of CD11b$^+$ and F4/80 cells**

For B16.F10 model: B16.F10 cancer cells (n=5) were subcutaneously injected (3e4) into the right hind flank of C57BL/6 mice. After approximately 22 days, mice bearing tumors greater than 1 cm were sacrificed. For APC model: APC mice were genotyped for *APC* mutation to confirmed homozygosity of transgene. At approximately 12-15 weeks of age, APC mice were sacrificed by cervical dislocation. The small intestine was removed from host and cut longitudinally, running parallel to the intestinal lining. Adenomas lining the intestine were excised using an open blade and pooled, respective to the host, in ice cold PBS supplemented with 0.5% (w/v) bovine serum albumin (BSA). For both model systems: once the tumor, spleen, and bone marrow were isolated from tumor bearing hosts, tissues were dissociated through enzymatic digestion (TrypLE) at 37°C for 30 min on a rocker 85 plate, followed by

cell straining through a 22 μm filter in ice cold PBS + 0.5% (w/v) BSA. Cell suspensions were then stained for $CD11b^+$ positivity by first using a CD11b-biotin conjugated antibody (BD Biosciences) and incubated for 15 min at 4°C. Cells were then washed twice with PBS + 0.5% BSA and positively selected by magnetic separation using a biotin isolation kit (Stem Cell) according to manufacturer's specifications. $F4/80^+$ macrophages were isolated from subcutaneous B16.ERAI tumors from the right hind flank *Ern1 x LysMCre* or *fl/fl* mice. After approximately 22 days, mice bearing tumors > 1 cm in length were sacrificed. Tumors and spleens were isolated, tissues were dissociated through enzymatic digestion (TrypLE) at 37°C for 30 min on a rocker 85 plate, followed by cell straining through a 22 μm filter in ice cold PBS + 0.5% (w/v) BSA. Cell suspensions were then stained for $F4/80^+$ positivity by first using a F4/80-PE conjugated antibody (StemCell Technologies Cat# 60027PE.1) and incubated for 15 min at 4°C. Cells were then washed twice with PBS 0.5% BSA and positively-selected by magnetic separation using PE Positive Selection Kit II (StemCell Technologies) according to manufacturer's specifications.

**RNASeq analysis**

RNA was extracted from wild type or Ern1 CKO BMDM that were untreated or treated with TERS CM for 18 hours using the Nucelospin RNA kit (Macherey Nagel). Each group consisted of 3 independently-derived BMDM. RNA sample purity was ascertained by the Nanodrop quantification method. Single end stranded RNA libraries for were sequenced on an Illumina HiSeq 4000. All samples and replicates were sequenced together on the same run. All 12 mouse RNA-seq transcript quantification was performed with sailfish version 0.9.2 [77], using the GRCm38 mouse transcriptome downloaded from Ensembl (URL: ftp://ftp.ensembl.org/pub/release-97/fasta/mus_musculus/cdna/Mus_musculus.GRCm38.cdna.all.fa.gz) with default parameters. The 33 RIDD target genes were collected from [49]. We z-scored these RIDD

target genes within each group separately (*Ern1* fl/fl and *Ern1* CKO) and then mean value was calculated and compared between different phenotype (untreated vs TERS CM treated) within each group.

**Ordinary Least Squares (OLS) linear model predicting PD-L1 using IRE1α pathway and PERK pathway downstream genes**

OLS models were fitted and compared using the python (version 2.7.15) statsmodels package (version 0.9.0). We collected IRE1α pathway (R-HSA-381070.1) and PERK pathway (R-HSA-381042.1) downstream genes from REACTOME [54]. Each gene was z-scored to ensure a mean of 0 and standard deviation of 1. Because quantification of transcript levels is noisier when genes are expressed at low levels, we implemented a filter to remove genes expressed under a certain threshold and evaluated pathway scores at thresholds ranging from 0 to 1000 reads. We then fitted models at different thresholds to evaluate robustness of the model to choice of threshold. Models were fitted using the formula:

$$PD - L1 = \beta_0 + \Sigma\beta_i \cdot gene_i$$

Nested OLS models with ERN1 only and ERN1 + PERK were compared using the Aikake information criterion (AIC). For each model, the AIC was calculated as AIC = $2k$ - $2\ln(L)$, where $k$ represents the number of estimated parameters, and $L$ represents the likelihood function for the model. Models were compared using the formula $\exp((AIC_{min} - AIC_i)/2)$, which represents the relative likelihood of model i with respect to the best available model.

**Statistical analysis**

To determine if differences between groups were statistically significant for PCR experiments, groups were compared using unpaired student's *t*-tests with Welch's correction. Statistically significant differences are indicated as follows: *p<0.05, **p<0.01, ***p<0.001,

649 ****p<0.0001. Statistical significance in tumor growth experiments was determined using the
650 Mann-Whitney *t* test and survival curves were generated by the Kaplan-Meier method.

651 **Acknowledgements**

652 This work was supported in part by grant RO1 CA220009 to M.Z. and H.C. J.J.R.
653 acknowledges the support of the Frank H. and Eva B. Buck Foundation. The authors thank
654 Valentina Ferrari for performing the QBeads assay.

655 **Author Contributions**

656 Conceptualization, M.Z., J.J.R., H.C., Reagents and Specimens, T.I., J.L., Data Collection,
657 A.B., J.J.R., S.X., S.S., A.L., G.A., K.J., Manuscript writing, M.Z., S.X, Manuscript
658 revisions, J.J.R., S.S., J.L., H.C., Supervision, J.J.R., H.C., M.Z. Funding acquisition, M.Z.,
659 H.C., J.J.R.

660 **Declaration of Interests**

661 All the other authors declare no conflict.

662

663

664

## Figure legends

**Figure 1. Activation of the UPR and acquisition of the IIS phenotype by tumor-infiltrating CD11b$^+$ cells *in vivo*.** (A) Flow cytometry histogram and comparative mean fluorescent intensity (MFI) values (n=4) of ERAI expression in CD11b$^+$ cells resident in specified tissue. (B,C) Gene expression in CD11b$^+$ cells isolated from B16.F10 tumors and respective bone marrow (n≥2 /group). Gene expression was arbitrarily normalized to one bone marrow sample and values represent relative quantification (RQ) fold transcription expression. (D,E) Gene expression in CD11b$^+$ cells isolated from APC adenomas, and respective bone marrow and spleen (n≥2 / group). RNA extracted from these cells was analyzed by RT-qPCR using specific primers.

**Figure 2. Chemical IRE1α inhibition prevents IIS polarization of BMDM *in vitro*.** BMDM were culture *in vitro* in conditioned medium of ER stressed cancer cells (TERS CM) for 18 hours with or without 4u8C (30 μM) and their mRNA subsequently tested by RT-qPCR to detect the expression of (A) UPR genes (Grp78 and Chop) (B) pro-inflammatory cytokines (*Il6* and *Il23p19*), and (C) immune suppression genes (*Arg1*) (n=3-5/group). Relative quantification (RQ) was determined by arbitrarily normalizing gene expression to a Vehicle CM condition. Data points are expressed as means ±SEM. (D) Flow cytometry analysis of the intracellular expression of Venus protein (ERAI), and CD86 and PD-L1 surface expression in BMDM treated with conditioned medium of ER stressed tumor cells (TERS CM) with or without 4u8C (30 μM).

685 **Figure 3. Deficiency in the IRE1α-XBP1 axis in macrophages attenuates the IIS**
686 **phenotype, PD-L1 expression and tumor growth.** (A) Western blot analysis of *Ern1* CKO
687 BMDM showing lack Ire1upon activation (24 hrs) by thapsigargin (Tg) (300 nM). (B)
688 Western blot analysis of *Ern1* CKO BMDM showing lack of spliced Xbp1 (Xbp1s) following
689 activation (24 hrs) by by thapsigargin (Tg) (300 nM). (C) Western blot analysis of *Xbp1* CKO
690 BMDM showing lack of spliced Xbp1 (Xbp1s) following activation (24 hrs) by thapsigargin
691 (Tg) (300 nM). (D) RT-qPCR analysis of UPR and IIS genes in wild type or CKO BMDM
692 untreated or treated with TERS CM . Values represent the mean ± SEM (n= 3-5/group). (E)
693 IRE1-XBP1 deficiency reduces CD86 and PD-L1 expression in BMDM. *Ern1*fl/fl, *Xbp1*fl/fl,
694 *Ern1* CKO and *Xbp1* CKO BMDM were treated (18 hrs) with TERS CM and subsequently
695 stained with PE-conjugated antibodies to CD86 and CD274. The MFI for both surface proteins
696 was quantified and plotted against the MFI of the corresponding unstimulated control. Statistical
697 significance was determined using the Mann-Whitney *t* test. (n=4-5 mice/group).

698 **Figure 4. Tumor growth and tumor-infiltrating macrophage analysis in *Ern1/Xbp1***
699 **conditional knock out mice**. (A) Kaplan-Meier survival curves of *Ern1fl/fl, Xbp1fl/fl, Ern1*
700 CKO and *Xbp1*CKO mice injected in the right flank with 3x10e4 B16.ERAI
701 cells/mouse. Tumor measurements were taken every two days in two dimensions. Mice
702 were sacrificed once tumors reached 20 mm in either dimension. (B) Gene expression in
703 F4/80$^{+}$ macrophages isolated from B16.F10 tumors implanted in *Ern1* CKO or *fl/fl* mice, and
704 respective spleen controls (n=2/group). mRNA was extracted enzymatically using the Zygem
705 RNAgem Tissue PLUS kit. Gene expression was arbitrarily normalized to one spleen sample
706 and values represent relative quantification fold transcript expression. Data points are
707 expressed as means ±SEM.

708 **Figure 5. RIDD analysis of wild type and *Ern1* CKO BMDM treated with TERS CM.**
709 (A) Fold change in *Cd247* (PD-L1) transcription in *Ern1* deficient (left panel) and *XBP1*
710 deficient (right panel) bone marrow-derived macrophages activated with TERS CM. (B)
711 RNASeq analysis of *Ern1* expression in untreated or TERS CM treated wild type or *Ern1*

712 CKO BMDM. TERS CM-induced fold changes are indicated in the graph. (C) Heatmap
713 showing te relative expression of 16 RIDD target genes in untreated or TERS CM-treated
714 wild type or *Ern1* CKO BMDM. (D) RNASeq analysis of *Cd274* expression in untreated or
715 TERS CM treated wild type or *Ern1* CKO BMDM. TERS CM-induced fold changes are
716 indicated in the graph. (E) Comparison of mean z-scores for the 16 RIDD target genes in
717 untreated or TERS CM-treated wild type or *Ern1* CKO BMDM.

718 **Figure 6. Ordinary least squares (OLS) linear model prediction of *CD274* gene**
719 **expression in human tumor associated macrophages**. (A) An illustration of the
720 development of aggregated pathway scores. For both pathways we used filters with different
721 thresholds to filter out genes with less read counts to account for baseline technical artifacts.
722 Then we z-score transformed both the gene matrix for both pathways and aggregated these
723 scores to predict *CD274* gene expression (B) RNAseq data from tumor associated
724 macrophages isolated from 13 human endometrial or breast cancer samples were analyzed
725 using 11 OLS linear models for each pathway (IRE1α or PERK). Each model was applied
726 using different filters, each representing increasing read count thresholds. In the upper panel
727 each dot represents the fraction of genes remaining in the model after a given filter was
728 applied. In the lower panel the *p* value for each pathway predicting PD-L1 gene expression is
729 indicated at each read count threshold.

730

731

732

733

734

## REFERENCES

1. Qian BZ, Pollard JW. Macrophage diversity enhances tumor progression and metastasis. Cell. 2010;141(1):39-51. Epub 2010/04/08. doi: S0092-8674(10)00287-4 [pii] 10.1016/j.cell.2010.03.014. PubMed PMID: 20371344.

2. Tlsty TD, Coussens LM. Tumor stroma and regulation of cancer development. Annu Rev Pathol. 2006;1:119-50. Epub 2007/11/28. doi: 10.1146/annurev.pathol.1.110304.100224. PubMed PMID: 18039110.

3. Sica A, Bronte V. Altered macrophage differentiation and immune dysfunction in tumor development. J Clin Invest. 2007;117(5):1155-66. Epub 2007/05/04. doi: 10.1172/JCI31422. PubMed PMID: 17476345; PubMed Central PMCID: PMC1857267.

4. Ostrand-Rosenberg S, Sinha P. Myeloid-derived suppressor cells: linking inflammation and cancer. J Immunol. 2009;182(8):4499-506. Epub 2009/04/04. doi: 182/8/4499 [pii] 10.4049/jimmunol.0802740. PubMed PMID: 19342621; PubMed Central PMCID: PMC2810498.

5. Kaneda MM, Messer KS, Ralainirina N, Li H, Leem C, Gorjestani S, et al. PI3Kgamma is a molecular switch that controls immune suppression. Nature. 2016. doi: 10.1038/nature19834. PubMed PMID: 27642729.

6. Chittezhath M, Dhillon MK, Lim JY, Laoui D, Shalova IN, Teo YL, et al. Molecular profiling reveals a tumor-promoting phenotype of monocytes and macrophages in human cancer progression. Immunity. 2014;41(5):815-29. doi: 10.1016/j.immuni.2014.09.014. PubMed PMID: 25453823.

758 7. Sousa S, Brion R, Lintunen M, Kronqvist P, Sandholm J, Monkkonen J, et al. Human
759 breast cancer cells educate macrophages toward the M2 activation status. Breast Cancer Res.
760 2015;17:101. Epub 2015/08/06. doi: 10.1186/s13058-015-0621-0. PubMed PMID:
761 26243145; PubMed Central PMCID: PMCPMC4531540.

762 8. Gabrilovich DI, Ostrand-Rosenberg S, Bronte V. Coordinated regulation of myeloid
763 cells by tumours. Nat Rev Immunol. 2012;12(4):253-68. Epub 2012/03/23. doi: nri3175 [pii]
764 10.1038/nri3175. PubMed PMID: 22437938.

765 9. Quail DF, Joyce JA. Microenvironmental regulation of tumor progression and
766 metastasis. Nat Med. 2013;19(11):1423-37. Epub 2013/11/10. doi: 10.1038/nm.3394.
767 PubMed PMID: 24202395; PubMed Central PMCID: PMCPMC3954707.

768 10. Colegio OR, Chu NQ, Szabo AL, Chu T, Rhebergen AM, Jairam V, et al. Functional
769 polarization of tumour-associated macrophages by tumour-derived lactic acid. Nature.
770 2014;513(7519):559-63. doi: 10.1038/nature13490. PubMed PMID: 25043024.

771 11. Hefetz-Sela S, Stein I, Klieger Y, Porat R, Sade-Feldman M, Zreik F, et al.
772 Acquisition of an immunosuppressive protumorigenic macrophage phenotype depending on
773 c-Jun phosphorylation. Proc Natl Acad Sci U S A. 2014;111(49):17582-7. doi:
774 10.1073/pnas.1409700111. PubMed PMID: 25422452; PubMed Central PMCID:
775 PMC4267378.

776 12. Condamine T, Dominguez GA, Youn JI, Kossenkov AV, Mony S, Alicea-Torres K, et
777 al. Lectin-type oxidized LDL receptor-1 distinguishes population of human
778 polymorphonuclear myeloid-derived suppressor cells in cancer patients. Sci Immunol.
779 2016;1(2). Epub 2017/04/19. doi: 10.1126/sciimmunol.aaf8943. PubMed PMID: 28417112;
780 PubMed Central PMCID: PMCPMC5391495.

781 13. Baer C, Squadrito ML, Laoui D, Thompson D, Hansen SK, Kiialainen A, et al.
782 Suppression of microRNA activity amplifies IFN-gamma-induced macrophage activation and
783 promotes anti-tumour immunity. Nat Cell Biol. 2016;18(7):790-802. Epub 2016/06/14. doi:
784 10.1038/ncb3371. PubMed PMID: 27295554.

785 14. Tavazoie MF, Pollack I, Tanqueco R, Ostendorf BN, Reis BS, Gonsalves FC, et al.
786 LXR/ApoE Activation Restricts Innate Immune Suppression in Cancer. Cell.
787 2018;172(4):825-40 e18. Epub 2018/01/18. doi: 10.1016/j.cell.2017.12.026. PubMed PMID:
788 29336888; PubMed Central PMCID: PMCPMC5846344.

789 15. Koumenis C. ER stress, hypoxia tolerance and tumor progression. Curr Mol Med.
790 2006;6(1):55-69. Epub 2006/02/14. PubMed PMID: 16472113.

791 16. Stewart B, Wild C. World Cancer Report 2014. Geneva: World Health Organization,
792 2014.

793 17. Weaver BA, Cleveland DW. The aneuploidy paradox in cell growth and
794 tumorigenesis. Cancer Cell. 2008;14(6):431-3. Epub 2008/12/09. doi:
795 10.1016/j.ccr.2008.11.011. PubMed PMID: 19061834; PubMed Central PMCID:
796 PMCPMC3132552.

797 18. Clarke HJ, Chambers JE, Liniker E, Marciniak SJ. Endoplasmic reticulum stress in
798 malignancy. Cancer Cell. 2014;25(5):563-73. doi: 10.1016/j.ccr.2014.03.015. PubMed
799 PMID: 24823636.

800 19. Wang M, Kaufman RJ. The impact of the endoplasmic reticulum protein-folding
801 environment on cancer development. Nat Rev Cancer. 2014;14(9):581-97. doi:
802 10.1038/nrc3800. PubMed PMID: 25145482.

803 20. Walter P, Ron D. The unfolded protein response: from stress pathway to homeostatic
804 regulation. Science. 2011;334(6059):1081-6. Epub 2011/11/26. doi: 334/6059/1081 [pii]

805 10.1126/science.1209038. PubMed PMID: 22116877.

806 21. Mori K. Signalling pathways in the unfolded protein response: development from
807 yeast to mammals. J Biochem. 2009;146(6):743-50. doi: 10.1093/jb/mvp166. PubMed
808 PMID: 19861400.

809 22. Schroder M, Kaufman RJ. ER stress and the unfolded protein response. Mutat Res.
810 2005;569(1-2):29-63. PubMed PMID: 15603751.

811 23. Martinon F, Chen X, Lee AH, Glimcher LH. TLR activation of the transcription
812 factor XBP1 regulates innate immune responses in macrophages. Nat Immunol.
813 2010;11(5):411-8. Epub 2010/03/31. doi: ni.1857 [pii]

814 10.1038/ni.1857. PubMed PMID: 20351694.

815 24. Hollien J, Weissman JS. Decay of endoplasmic reticulum-localized mRNAs during
816 the unfolded protein response. Science. 2006;313(5783):104-7. doi:
817 10.1126/science.1129631. PubMed PMID: 16825573.

818 25. Yoshida H, Matsui T, Yamamoto A, Okada T, Mori K. XBP1 mRNA is induced by
819 ATF6 and spliced by IRE1 in response to ER stress to produce a highly active transcription
820 factor. Cell. 2001;107(7):881-91. Epub 2002/01/10. doi: S0092-8674(01)00611-0 [pii].
821 PubMed PMID: 11779464.

822 26. Mahadevan NR, Rodvold J, Sepulveda H, Rossi S, Drew AF, Zanetti M.
823 Transmission of endoplasmic reticulum stress and pro-inflammation from tumor cells to
824 myeloid cells. Proc Natl Acad Sci U S A. 2011;108(16):6561-6. Epub 2011/04/06. doi:
825 1008942108 [pii]

826 10.1073/pnas.1008942108. PubMed PMID: 21464300; PubMed Central PMCID:
827 PMC3081038.

828 27. Rodvold JJ, Chiu KT, Hiramatsu N, Nussbacher JK, Galimberti V, Mahadevan NR, et
829 al. Intercellular transmission of the unfolded protein response promotes survival and drug
830 resistance in cancer cells. Sci Signal. 2017;10(482). Epub 2017/06/08. doi:
831 10.1126/scisignal.aah7177. PubMed PMID: 28588081.

832 28. Mahadevan NR, Anufreichik V, Rodvold JJ, Chiu KT, Sepulveda H, Zanetti M. Cell-
833 Extrinsic Effects of Tumor ER Stress Imprint Myeloid Dendritic Cells and Impair CD8(+) T
834 Cell Priming. PLoS One. 2012;7(12):e51845. Epub 2012/12/29. doi:
835 10.1371/journal.pone.0051845

836 PONE-D-12-20796 [pii]. PubMed PMID: 23272178; PubMed Central PMCID:
837 PMC3525659.

838 29. Axelrod R, Axelrod DE, Pienta KJ. Evolution of cooperation among tumor cells. Proc
839 Natl Acad Sci U S A. 2006;103(36):13474-9. doi: 10.1073/pnas.0606053103. PubMed
840 PMID: 16938860; PubMed Central PMCID: PMC1557388.

841 30. Gurdon JB, Lemaire P, Kato K. Community effects and related phenomena in
842 development. Cell. 1993;75(5):831-4. PubMed PMID: 8252618.

843 31. Jouanneau J, Moens G, Bourgeois Y, Poupon MF, Thiery JP. A minority of
844 carcinoma cells producing acidic fibroblast growth factor induces a community effect for
845 tumor progression. Proc Natl Acad Sci U S A. 1994;91(1):286-90. PubMed PMID: 7506417;
846 PubMed Central PMCID: PMC42932.

847 32. Kim S, Takahashi H, Lin WW, Descargues P, Grivennikov S, Kim Y, et al.
848 Carcinoma-produced factors activate myeloid cells through TLR2 to stimulate metastasis.
849 Nature. 2009;457(7225):102-6. Epub 2009/01/06. doi: nature07623 [pii]

850 10.1038/nature07623. PubMed PMID: 19122641.

851 33. Grivennikov S, Karin E, Terzic J, Mucida D, Yu GY, Vallabhapurapu S, et al. IL-6
852 and Stat3 are required for survival of intestinal epithelial cells and development of colitis-
853 associated cancer. Cancer Cell. 2009;15(2):103-13. doi: 10.1016/j.ccr.2009.01.001. PubMed
854 PMID: 19185845; PubMed Central PMCID: PMC2667107.

855 34. Langowski JL, Zhang X, Wu L, Mattson JD, Chen T, Smith K, et al. IL-23 promotes
856 tumour incidence and growth. Nature. 2006;442(7101):461-5. PubMed PMID: 16688182.

857 35. Norian LA, Rodriguez PC, O'Mara LA, Zabaleta J, Ochoa AC, Cella M, et al. Tumor-
858 infiltrating regulatory dendritic cells inhibit CD8+ T cell function via L-arginine metabolism.
859 Cancer Res. 2009;69(7):3086-94. Epub 2009/03/19. doi: 0008-5472.CAN-08-2826 [pii]

860 10.1158/0008-5472.CAN-08-2826. PubMed PMID: 19293186; PubMed Central PMCID:
861 PMC2848068.

862 36. Cubillos-Ruiz JR, Silberman PC, Rutkowski MR, Chopra S, Perales-Puchalt A, Song
863 M, et al. ER Stress Sensor XBP1 Controls Anti-tumor Immunity by Disrupting Dendritic Cell
864 Homeostasis. Cell. 2015;161(7):1527-38. doi: 10.1016/j.cell.2015.05.025. PubMed PMID:
865 26073941.

866 37. Cook KL, Soto-Pantoja DR, Clarke PA, Cruz MI, Zwart A, Warri A, et al.
867 Endoplasmic Reticulum Stress Protein GRP78 Modulates Lipid Metabolism to Control Drug
868 Sensitivity and Antitumor Immunity in Breast Cancer. Cancer Res. 2016;76(19):5657-70.
869 Epub 2016/10/05. doi: 10.1158/0008-5472.CAN-15-2616. PubMed PMID: 27698188;
870 PubMed Central PMCID: PMCPMC5117832.

871 38. Gentles AJ, Newman AM, Liu CL, Bratman SV, Feng W, Kim D, et al. The
872 prognostic landscape of genes and infiltrating immune cells across human cancers. Nat Med.
873 2015;21(8):938-45. doi: 10.1038/nm.3909. PubMed PMID: 26193342.

874 39. Condamine T, Kumar V, Ramachandran IR, Youn JI, Celis E, Finnberg N, et al. ER
875 stress regulates myeloid-derived suppressor cell fate through TRAIL-R-mediated apoptosis. J
876 Clin Invest. 2014;124(6):2626-39. doi: 10.1172/JCI74056. PubMed PMID: 24789911;
877 PubMed Central PMCID: PMC4038578.

878 40. Osorio F, Tavernier SJ, Hoffmann E, Saeys Y, Martens L, Vetters J, et al. The
879 unfolded-protein-response sensor IRE-1alpha regulates the function of CD8alpha(+) dendritic
880 cells. Nat Immunol. 2014;15(3):248-57. doi: 10.1038/ni.2808. PubMed PMID: 24441789.

881 41. Iwawaki T, Akai R, Kohno K, Miura M. A transgenic mouse model for monitoring
882 endoplasmic reticulum stress. Nat Med. 2004;10(1):98-102. PubMed PMID: 14702639.

883 42. Moser AR, Luongo C, Gould KA, McNeley MK, Shoemaker AR, Dove WF.
884 ApcMin: a mouse model for intestinal and mammary tumorigenesis. Eur J Cancer.
885 1995;31A(7-8):1061-4. Epub 1995/07/01. PubMed PMID: 7576992.

886 43. Axten JM, Romeril SP, Shu A, Ralph J, Medina JR, Feng Y, et al. Discovery of
887 GSK2656157: An Optimized PERK Inhibitor Selected for Preclinical Development. ACS
888 Med Chem Lett. 2013;4(10):964-8. doi: 10.1021/ml400228e. PubMed PMID: 24900593;
889 PubMed Central PMCID: PMCPMC4027568.

890 44. Iwakoshi NN, Pypaert M, Glimcher LH. The transcription factor XBP-1 is essential
891 for the development and survival of dendritic cells. J Exp Med. 2007;204(10):2267-75. Epub
892 2007/09/19. doi: jem.20070525 [pii]

893 10.1084/jem.20070525. PubMed PMID: 17875675; PubMed Central PMCID: PMC2118458.

894 45. Tavernier SJ, Osorio F, Vandersarren L, Vetters J, Vanlangenakker N, Van Isterdael
895 G, et al. Regulated IRE1-dependent mRNA decay sets the threshold for dendritic cell
896 survival. Nat Cell Biol. 2017;19(6):698-710. Epub 2017/05/02. doi: 10.1038/ncb3518.
897 PubMed PMID: 28459443; PubMed Central PMCID: PMCPMC5563826.

898 46. Cross BC, Bond PJ, Sadowski PG, Jha BK, Zak J, Goodman JM, et al. The molecular
899 basis for selective inhibition of unconventional mRNA splicing by an IRE1-binding small
900 molecule. Proc Natl Acad Sci U S A. 2012;109(15):E869-78. doi: 10.1073/pnas.1115623109.
901 PubMed PMID: 22315414; PubMed Central PMCID: PMC3326519.

902 47. Hetz C, Lee AH, Gonzalez-Romero D, Thielen P, Castilla J, Soto C, et al. Unfolded
903 protein response transcription factor XBP-1 does not influence prion replication or
904 pathogenesis. Proc Natl Acad Sci U S A. 2008;105(2):757-62. Epub 2008/01/08. doi:
905 0711094105 [pii]

906 10.1073/pnas.0711094105. PubMed PMID: 18178615; PubMed Central PMCID:
907 PMC2206609.

908 48. Clausen BE, Burkhardt C, Reith W, Renkawitz R, Forster I. Conditional gene
909 targeting in macrophages and granulocytes using LysMcre mice. Transgenic Res.
910 1999;8(4):265-77. Epub 2000/01/06. PubMed PMID: 10621974.

911 49. Maurel M, Chevet E, Tavernier J, Gerlo S. Getting RIDD of RNA: IRE1 in cell fate
912 regulation. Trends Biochem Sci. 2014. doi: 10.1016/j.tibs.2014.02.008. PubMed PMID:
913 24657016.

914 50. Howarth M, Williams A, Tolstrup AB, Elliott T. Tapasin enhances MHC class I
915 peptide presentation according to peptide half-life. Proc Natl Acad Sci U S A.
916 2004;101(32):11737-42. PubMed PMID: 15286279.

917 51. Xu Y, Poggio M, Jin HY, Shi Z, Forester CM, Wang Y, et al. Translation control of
918 the immune checkpoint in cancer and its therapeutic targeting. Nat Med. 2019;25(2):301-11.
919 Epub 2019/01/16. doi: 10.1038/s41591-018-0321-2. PubMed PMID: 30643286; PubMed
920 Central PMCID: PMCPMC6613562.

921 52. Cassetta L, Fragkogianni S, Sims AH, Swierczak A, Forrester LM, Zhang H, et al.
922 Human Tumor-Associated Macrophage and Monocyte Transcriptional Landscapes Reveal
923 Cancer-Specific Reprogramming, Biomarkers, and Therapeutic Targets. Cancer Cell.
924 2019;35(4):588-602 e10. Epub 2019/04/02. doi: 10.1016/j.ccell.2019.02.009. PubMed PMID:
925 30930117; PubMed Central PMCID: PMCPMC6472943.

926 53. Adams CJ, Kopp MC, Larburu N, Nowak PR, Ali MMU. Structure and Molecular
927 Mechanism of ER Stress Signaling by the Unfolded Protein Response Signal Activator IRE1.
928 Front Mol Biosci. 2019;6:11. Epub 2019/04/02. doi: 10.3389/fmolb.2019.00011. PubMed
929 PMID: 30931312; PubMed Central PMCID: PMCPMC6423427.

930 54. Fabregat A, Jupe S, Matthews L, Sidiropoulos K, Gillespie M, Garapati P, et al. The
931 Reactome Pathway Knowledgebase. Nucleic Acids Res. 2018;46(D1):D649-D55. Epub
932 2017/11/18. doi: 10.1093/nar/gkx1132. PubMed PMID: 29145629; PubMed Central PMCID:
933 PMCPMC5753187.

934 55. Cassetta L, Pollard JW. Targeting macrophages: therapeutic approaches in cancer.
935 Nat Rev Drug Discov. 2018;17(12):887-904. Epub 2018/10/27. doi: 10.1038/nrd.2018.169.
936 PubMed PMID: 30361552.

937 56. Van Ginderachter JA, Movahedi K, Hassanzadeh Ghassabeh G, Meerschaut S,
938 Beschin A, Raes G, et al. Classical and alternative activation of mononuclear phagocytes:
939 picking the best of both worlds for tumor promotion. Immunobiology. 2006;211(6-8):487-
940 501. Epub 2006/08/22. doi: S0171-2985(06)00082-9 [pii]

941 10.1016/j.imbio.2006.06.002. PubMed PMID: 16920488.

942 57. Mahadevan NR, Zanetti M. Tumor stress inside out: Cell-extrinsic effects of the
943 unfolded protein response in tumor cells modulate the immunological landscape of the tumor
944 microenvironment. J Immunol. 2011;187(9):4403-9. Epub 2011/10/21. doi: 187/9/4403 [pii]

945 10.4049/jimmunol.1101531. PubMed PMID: 22013206.

946 58. Junjappa RP, Patil P, Bhattarai KR, Kim HR, Chae HJ. IRE1alpha Implications in
947 Endoplasmic Reticulum Stress-Mediated Development and Pathogenesis of Autoimmune
948 Diseases. Front Immunol. 2018;9:1289. Epub 2018/06/22. doi: 10.3389/fimmu.2018.01289.
949 PubMed PMID: 29928282; PubMed Central PMCID: PMCPMC5997832.

950 59. Shan B, Wang X, Wu Y, Xu C, Xia Z, Dai J, et al. The metabolic ER stress sensor
951 IRE1alpha suppresses alternative activation of macrophages and impairs energy expenditure
952 in obesity. Nat Immunol. 2017;18(5):519-29. Epub 2017/03/28. doi: 10.1038/ni.3709.
953 PubMed PMID: 28346409.

954 60. Robblee MM, Kim CC, Porter Abate J, Valdearcos M, Sandlund KL, Shenoy MK, et
955 al. Saturated Fatty Acids Engage an IRE1alpha-Dependent Pathway to Activate the NLRP3
956 Inflammasome in Myeloid Cells. Cell Rep. 2016;14(11):2611-23. Epub 2016/03/15. doi:
957 10.1016/j.celrep.2016.02.053. PubMed PMID: 26971994; PubMed Central PMCID:
958 PMCPMC5242525.

959 61. Nish SA, Schenten D, Wunderlich FT, Pope SD, Gao Y, Hoshi N, et al. T cell-
960 intrinsic role of IL-6 signaling in primary and memory responses. Elife. 2014;3:e01949. Epub
961 2014/05/21. doi: 10.7554/eLife.01949. PubMed PMID: 24842874; PubMed Central PMCID:
962 PMCPMC4046568.

963 62. Yang R, Masters AR, Fortner KA, Champagne DP, Yanguas-Casas N, Silberger DJ,
964 et al. IL-6 promotes the differentiation of a subset of naive CD8+ T cells into IL-21-
965 producing B helper CD8+ T cells. J Exp Med. 2016;213(11):2281-91. Epub 2016/11/05. doi:
966 10.1084/jem.20160417. PubMed PMID: 27670591; PubMed Central PMCID:
967 PMCPMC5068236.

968 63. Li B, Jones LL, Geiger TL. IL-6 Promotes T Cell Proliferation and Expansion under
969 Inflammatory Conditions in Association with Low-Level RORgammat Expression. J
970 Immunol. 2018;201(10):2934-46. Epub 2018/10/14. doi: 10.4049/jimmunol.1800016.
971 PubMed PMID: 30315140; PubMed Central PMCID: PMCPMC6324200.

972 64. Aggarwal S, Ghilardi N, Xie MH, de Sauvage FJ, Gurney AL. Interleukin-23
973 promotes a distinct CD4 T cell activation state characterized by the production of interleukin-
974 17. J Biol Chem. 2003;278(3):1910-4. Epub 2002/11/06. doi: 10.1074/jbc.M207577200.
975 PubMed PMID: 12417590.

976 65. Revu S, Wu J, Henkel M, Rittenhouse N, Menk A, Delgoffe GM, et al. IL-23 and IL-
977 1beta Drive Human Th17 Cell Differentiation and Metabolic Reprogramming in Absence of
978 CD28 Costimulation. Cell Rep. 2018;22(10):2642-53. Epub 2018/03/08. doi:
979 10.1016/j.celrep.2018.02.044. PubMed PMID: 29514093; PubMed Central PMCID:
980 PMCPMC5884137.

981 66. Sun C, Mezzadra R, Schumacher TN. Regulation and Function of the PD-L1
982 Checkpoint. Immunity. 2018;48(3):434-52. Epub 2018/03/22. doi:
983 10.1016/j.immuni.2018.03.014. PubMed PMID: 29562194.

984 67. Lin H, Wei S, Hurt EM, Green MD, Zhao L, Vatan L, et al. Host expression of PD-L1
985 determines efficacy of PD-L1 pathway blockade-mediated tumor regression. J Clin Invest.
986 2018;128(2):805-15. Epub 2018/01/18. doi: 10.1172/JCI96113. PubMed PMID: 29337305;
987 PubMed Central PMCID: PMCPMC5785251.

988 68. Tang H, Liang Y, Anders RA, Taube JM, Qiu X, Mulgaonkar A, et al. PD-L1 on host
989 cells is essential for PD-L1 blockade-mediated tumor regression. J Clin Invest.
990 2018;128(2):580-8. Epub 2018/01/18. doi: 10.1172/JCI96061. PubMed PMID: 29337303;
991 PubMed Central PMCID: PMCPMC5785245.

992 69. Ahmadzadeh M, Johnson LA, Heemskerk B, Wunderlich JR, Dudley ME, White DE,
993 et al. Tumor antigen-specific CD8 T cells infiltrating the tumor express high levels of PD-1
994 and are functionally impaired. Blood. 2009;114(8):1537-44. doi: 10.1182/blood-2008-12-
995 195792. PubMed PMID: 19423728; PubMed Central PMCID: PMC2927090.

996 70. Kamada T, Togashi Y, Tay C, Ha D, Sasaki A, Nakamura Y, et al. PD-1(+)
997 regulatory T cells amplified by PD-1 blockade promote hyperprogression of cancer. Proc
998 Natl Acad Sci U S A. 2019;116(20):9999-10008. Epub 2019/04/28. doi:
999 10.1073/pnas.1822001116. PubMed PMID: 31028147; PubMed Central PMCID:
1000 PMCPMC6525547.

1001 71. Upton JP, Wang L, Han D, Wang ES, Huskey NE, Lim L, et al. IRE1alpha cleaves
1002 select microRNAs during ER stress to derepress translation of proapoptotic Caspase-2.
1003 Science. 2012;338(6108):818-22. doi: 10.1126/science.1226191. PubMed PMID: 23042294;
1004 PubMed Central PMCID: PMC3742121.

1005 72. Wang JM, Qiu Y, Yang Z, Kim H, Qian Q, Sun Q, et al. IRE1alpha prevents hepatic
1006 steatosis by processing and promoting the degradation of select microRNAs. Sci Signal.
1007 2018;11(530). Epub 2018/05/17. doi: 10.1126/scisignal.aao4617. PubMed PMID: 29764990;
1008 PubMed Central PMCID: PMCPMC6075656.

1009 73. Wang X, Li J, Dong K, Lin F, Long M, Ouyang Y, et al. Tumor suppressor miR-34a
1010 targets PD-L1 and functions as a potential immunotherapeutic target in acute myeloid
1011 leukemia. Cell Signal. 2015;27(3):443-52. Epub 2014/12/17. doi:
1012 10.1016/j.cellsig.2014.12.003. PubMed PMID: 25499621.

1013 74. Cortez MA, Ivan C, Valdecanas D, Wang X, Peltier HJ, Ye Y, et al. PDL1 Regulation
1014 by p53 via miR-34. J Natl Cancer Inst. 2016;108(1). Epub 2015/11/19. doi:

1015 10.1093/jnci/djv303. PubMed PMID: 26577528; PubMed Central PMCID:
1016 PMCPMC4862407.

1017 75. Sun J, Liu Y, Aballay A. Organismal regulation of XBP-1-mediated unfolded protein
1018 response during development and immune activation. EMBO Rep. 2012;13(9):855-60. doi:
1019 10.1038/embor.2012.100. PubMed PMID: 22791024; PubMed Central PMCID:
1020 PMC3432796.

1021 76. Taylor RC, Dillin A. XBP-1 Is a Cell-Nonautonomous Regulator of Stress Resistance
1022 and Longevity. Cell. 2013;153(7):1435-47. doi: 10.1016/j.cell.2013.05.042. PubMed PMID:
1023 23791175.

1024 77. Patro R, Mount SM, Kingsford C. Sailfish enables alignment-free isoform
1025 quantification from RNA-seq reads using lightweight algorithms. Nat Biotechnol.
1026 2014;32(5):462-4. doi: 10.1038/nbt.2862. PubMed PMID: 24752080; PubMed Central
1027 PMCID: PMC4077321.

1028

A

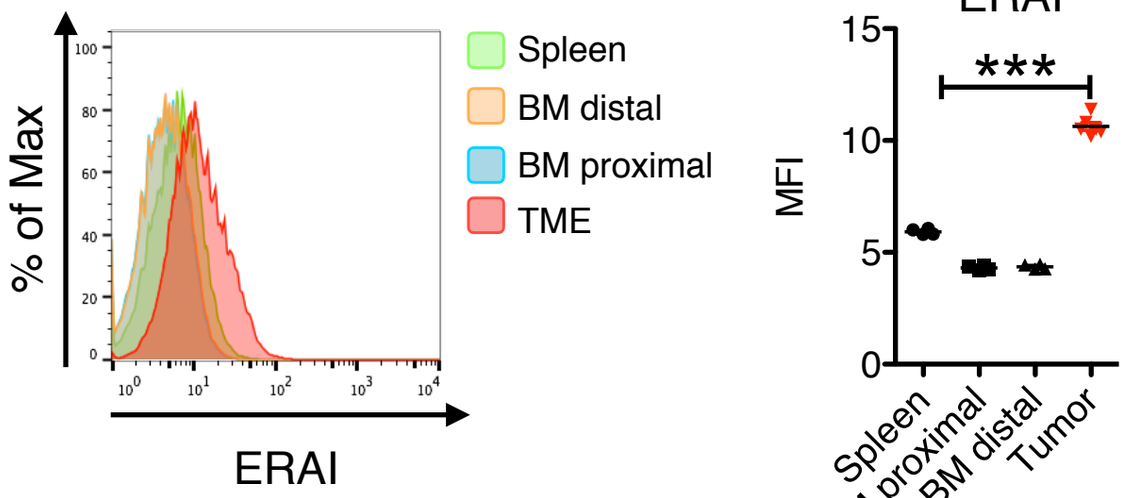
% of Max
ERAI
Spleen
BM distal
BM proximal
TME


ERAI
MFI
***
Spleen
BM proximal
BM distal
Tumor

B

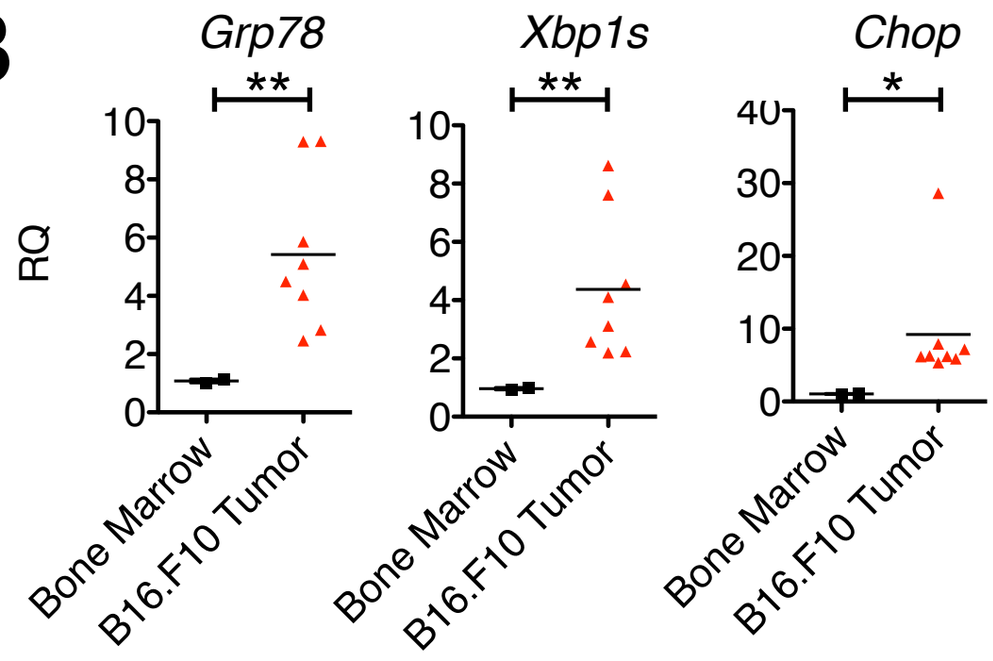
Grp78
Xbp1s
Chop
RQ
**
**
*
Bone Marrow
B16.F10 Tumor

C

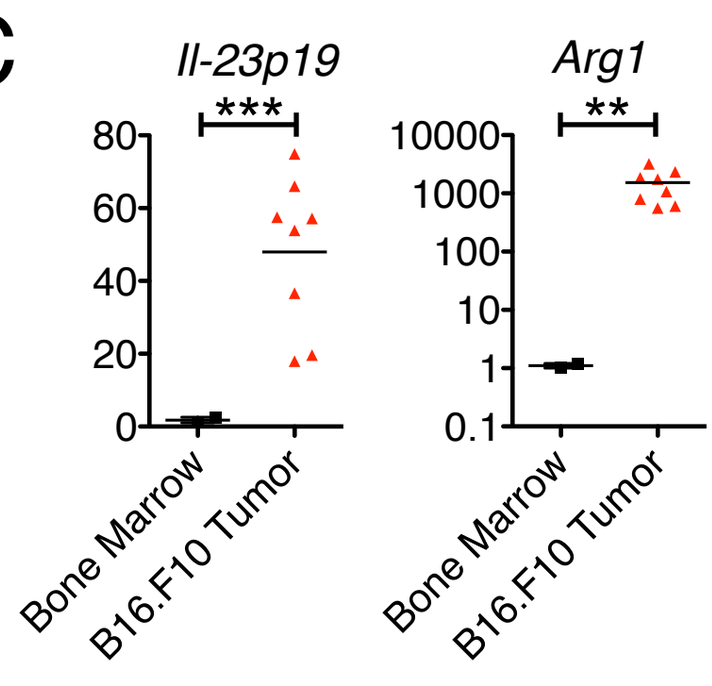
Il-23p19
Arg1
***
**
Bone Marrow
B16.F10 Tumor

D

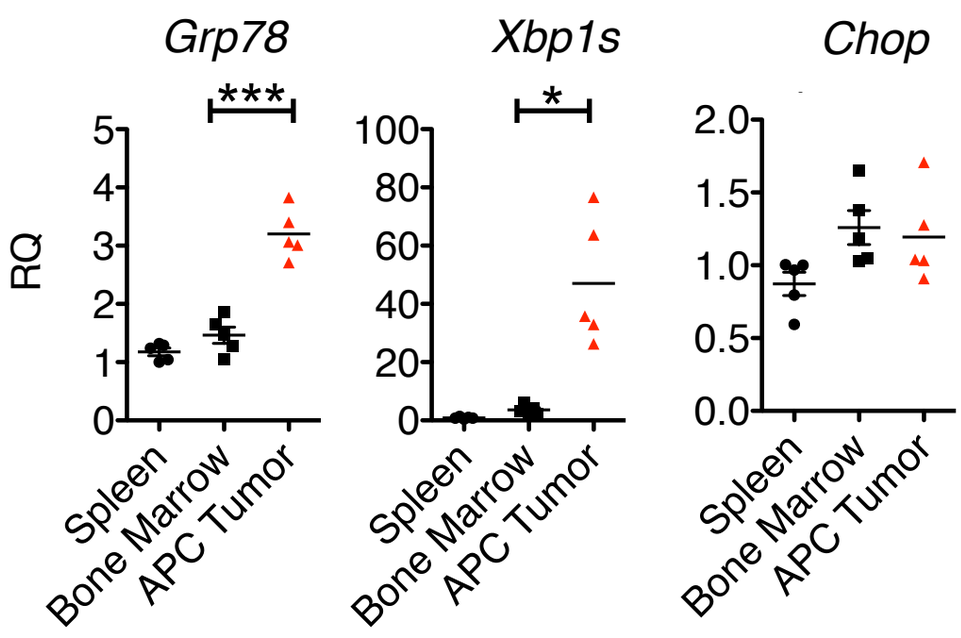
Grp78
Xbp1s
Chop
RQ
***
*
Spleen
Bone Marrow
APC Tumor

E

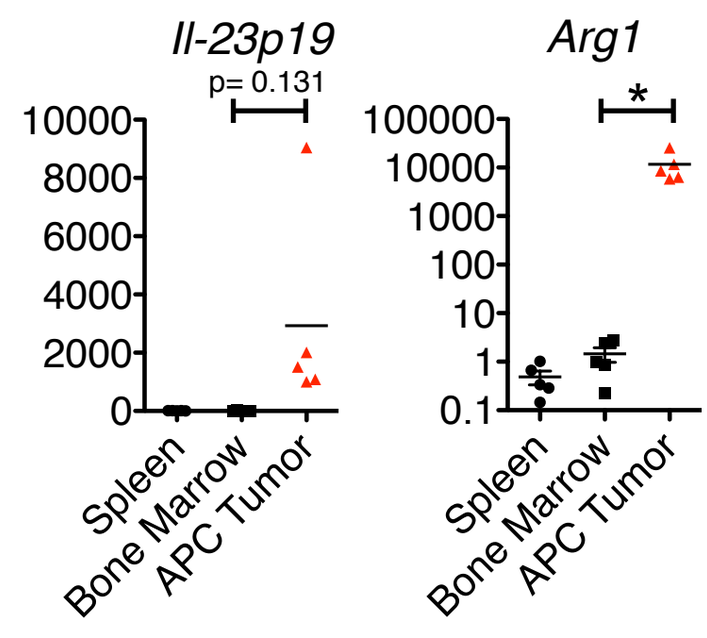
Il-23p19
Arg1
p= 0.131
*
Spleen
Bone Marrow
APC Tumor

Fig 1.

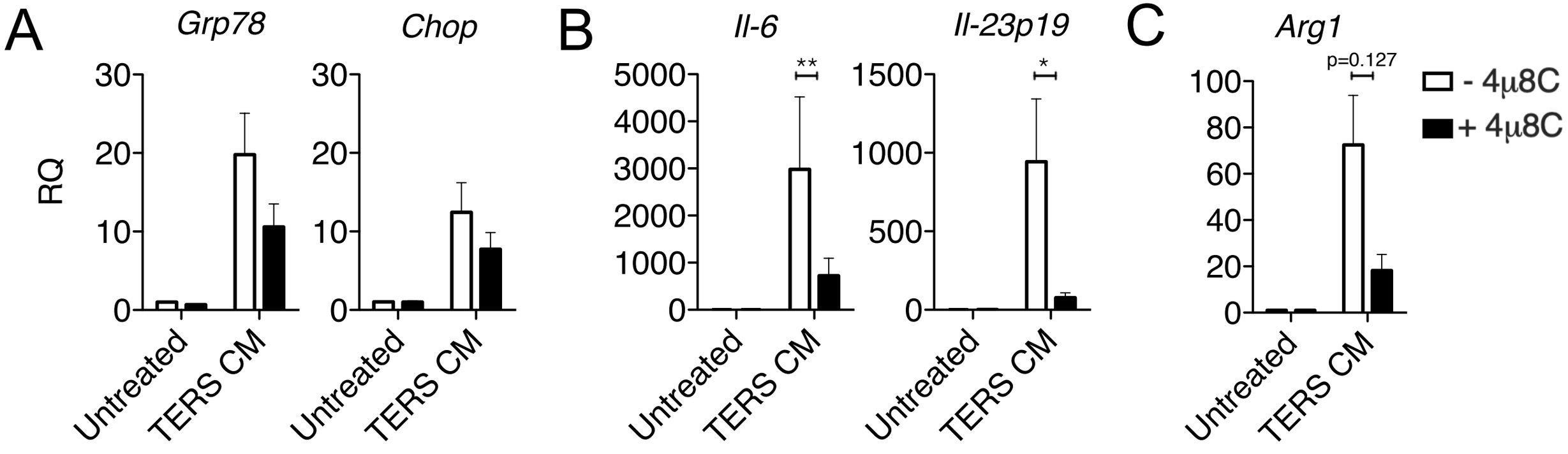
A
Grp78
Chop
RQ
30
20
10
0
Untreated
TERS CM
B
Il-6
Il-23p19
5000
4000
3000
2000
1000
1500
500
**
*
C
Arg1
p=0.127
100
80
60
40
- 4μ8C
+ 4μ8C
D
CD86
PD-L1
Δ MFI
300
200
- 4μ8C
+ 4μ8C

Fig 2.

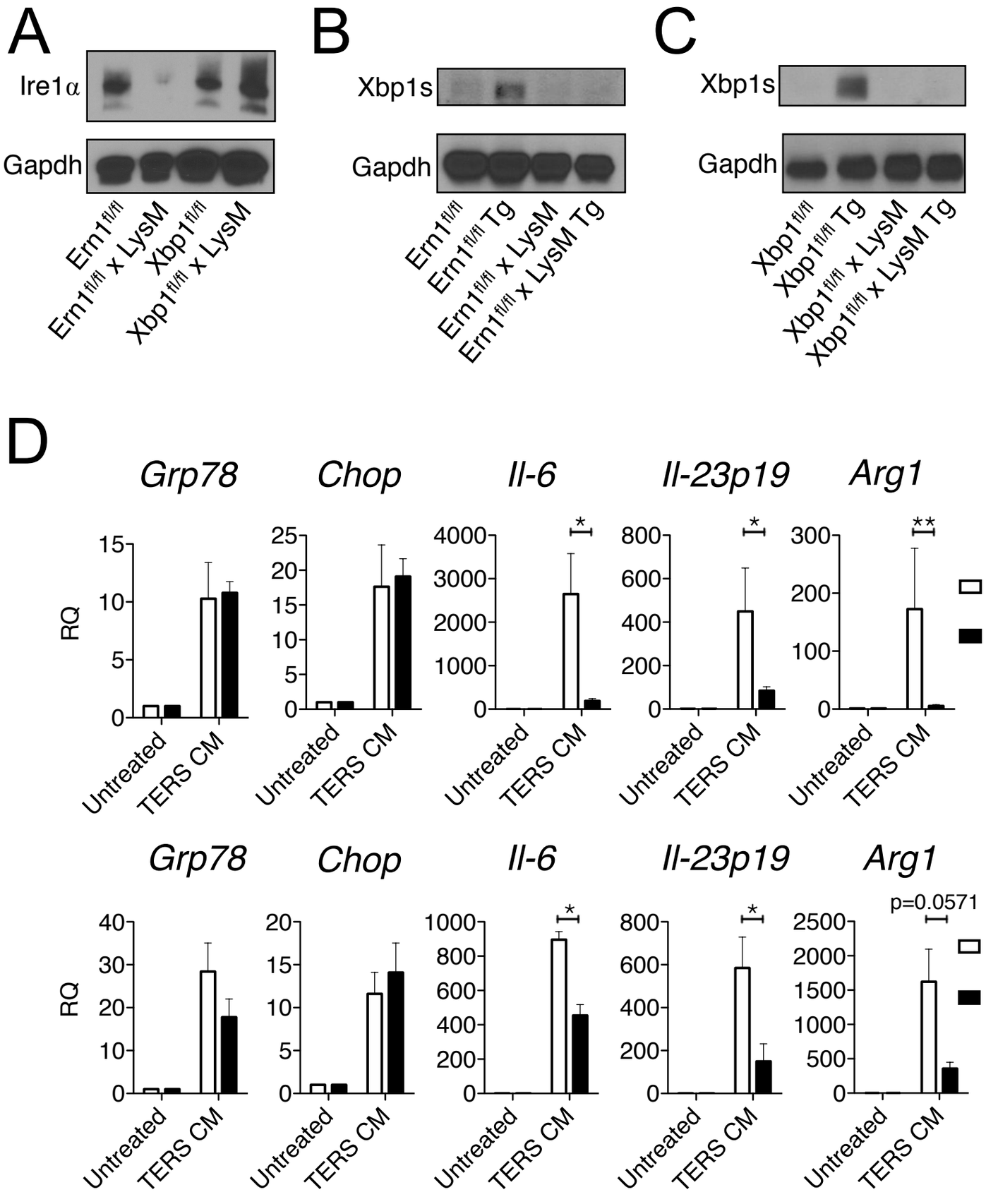
A
Ire1α
Gapdh
Ern1fl/fl
Ern1fl/fl x LysM
Xbp1fl/fl
Xbp1fl/fl x LysM
B
Xbp1s
Gapdh
Ern1fl/fl
Ern1fl/fl Tg
Ern1fl/fl x LysM
Ern1fl/fl x LysM Tg
C
Xbp1s
Gapdh
Xbp1fl/fl
Xbp1fl/fl Tg
Xbp1fl/fl x LysM
Xbp1fl/fl x LysM Tg
D
Grp78
Chop
Il-6
Il-23p19
Arg1
RQ
Untreated
TERS CM
Ern1 fl/fl
Ern1 x LysM
Xbp1 fl/fl
Xbp1 x LysM
p=0.0571
E
CD86 MFI
PD-L1 MFI
Ern1fl/fl
Ern1LysMCre
Xbp1fl/fl
Xbp1LysMCre
Untreated
TERS CM

Fig 3.

A

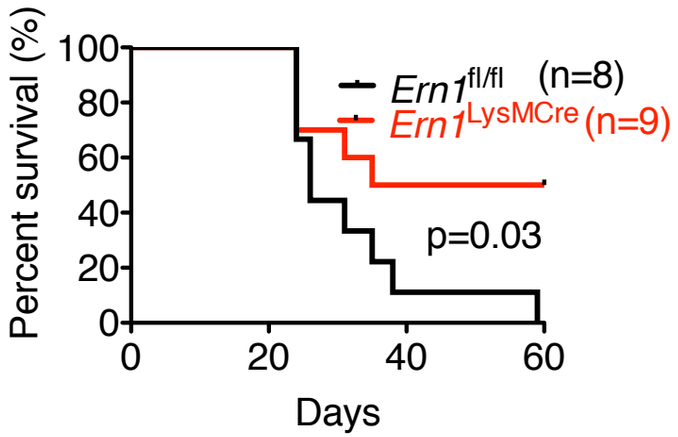
Percent survival (%)
100
80
60
40
20
0
0
20
40
60
Days
Ern1fl/fl (n=8)
Ern1LysMCre (n=9)
p=0.03

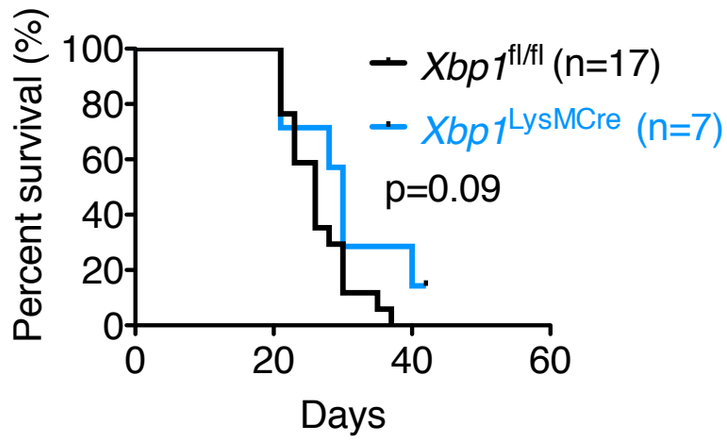
Percent survival (%)
100
80
60
40
20
0
0
20
40
60
Days
Xbp1fl/fl (n=17)
Xbp1LysMCre (n=7)
p=0.09

B

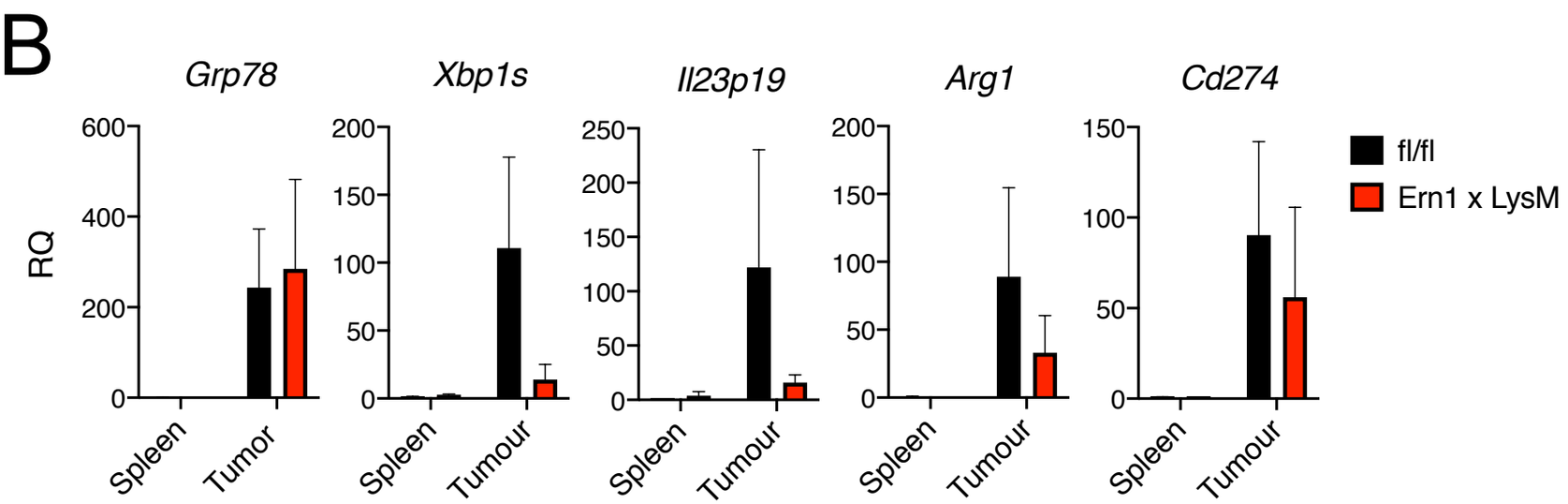
Grp78
Xbp1s
Il23p19
Arg1
Cd274
RQ
600
400
200
0
150
100
50
250
200
150
100
50
Spleen
Tumor
Tumour
fl/fl
Ern1 x LysM

Fig 4.

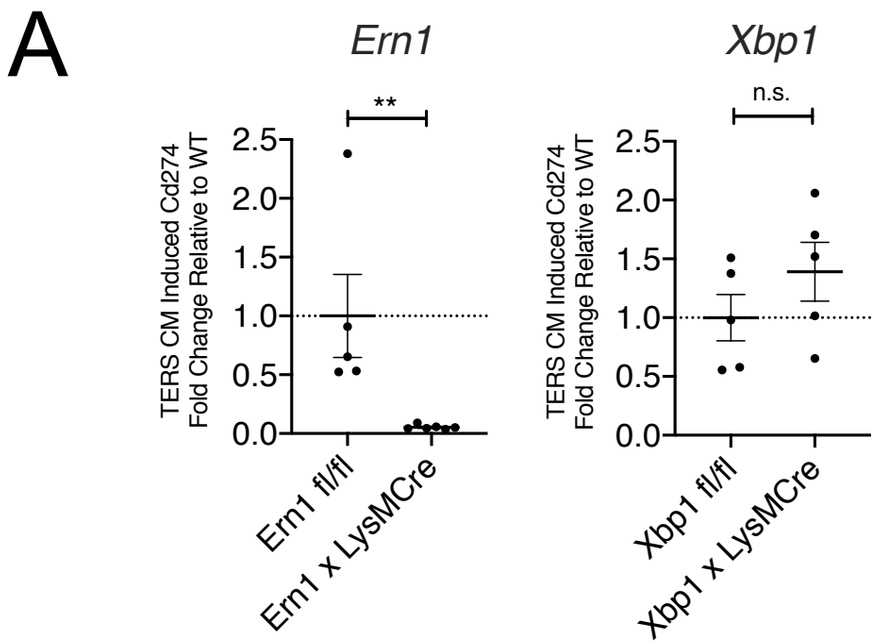
A
Ern1
Xbp1
**
n.s.
TERS CM Induced Cd274
Fold Change Relative to WT
2.5
2.0
1.5
1.0
0.5
0.0
Ern1 fl/fl
Ern1 x LysMCre
Xbp1 fl/fl
Xbp1 x LysMCre

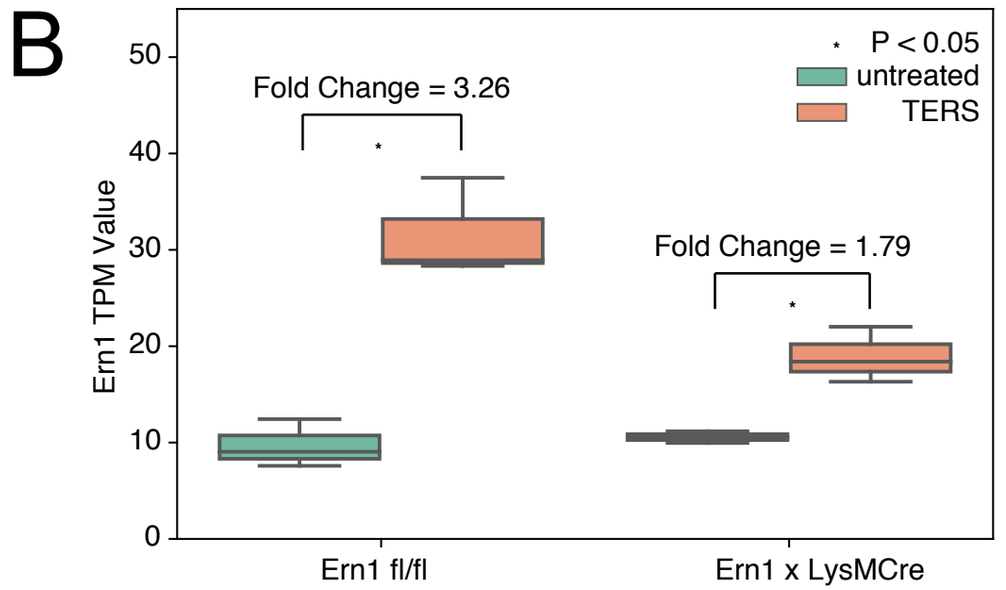
B
Ern1 TPM Value
50
40
30
20
10
0
Fold Change = 3.26
Fold Change = 1.79
P < 0.05
untreated
TERS
Ern1 fl/fl
Ern1 x LysMCre

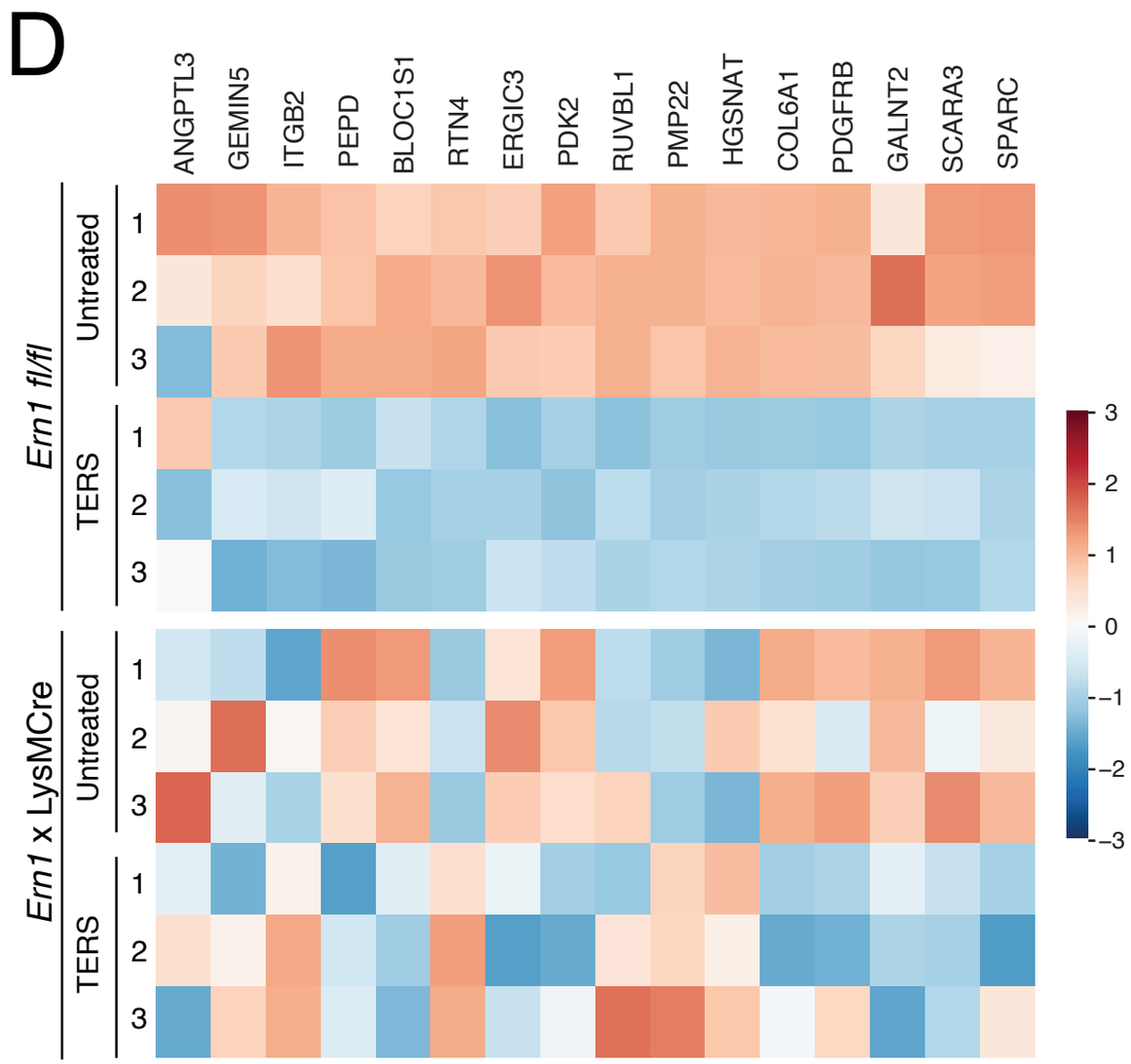
D
ANGPTL3
GEMIN5
ITGB2
PEPD
BLOC1S1
RTN4
ERGIC3
PDK2
RUVBL1
PMP22
HGSNAT
COL6A1
PDGFRB
GALNT2
SCARA3
SPARC
Ern1 fl/fl
Untreated
TERS
Ern1 x LysMCre
1
2
3
3
2
1
0
−1
−2
−3

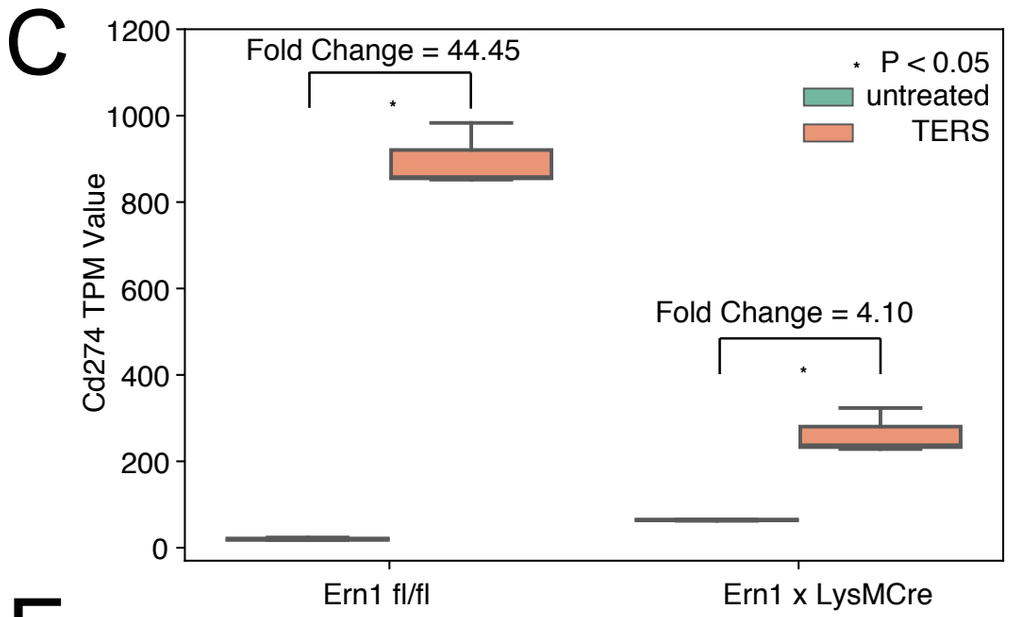
C
Cd274 TPM Value
1200
1000
800
600
400
200
0
Fold Change = 44.45
Fold Change = 4.10
P < 0.05
untreated
TERS
Ern1 fl/fl
Ern1 x LysMCre

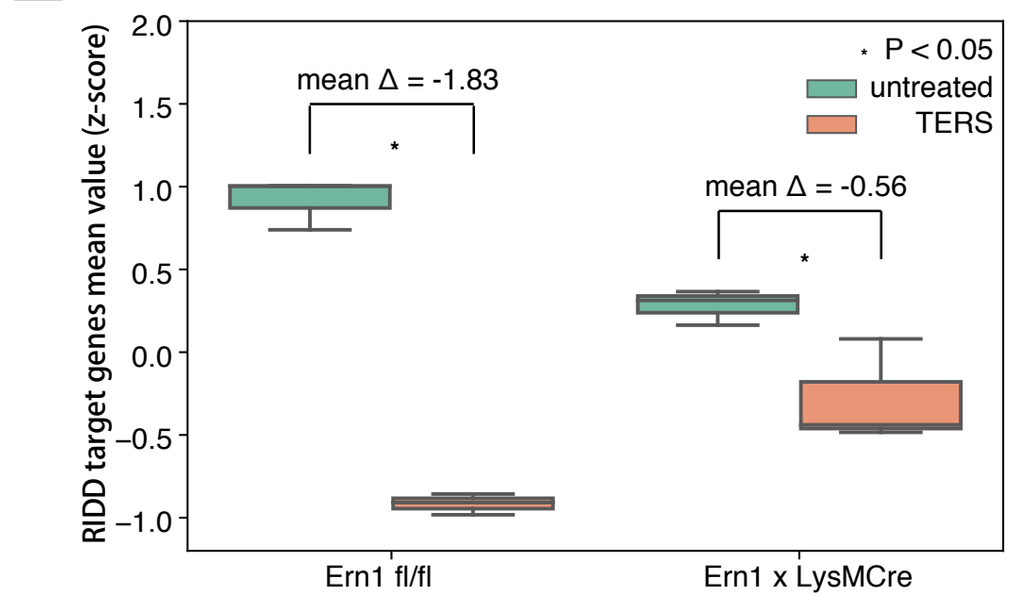
E
RIDD target genes mean value (z-score)
2.0
1.5
1.0
0.5
0.0
−0.5
−1.0
mean Δ = -1.83
mean Δ = -0.56
P < 0.05
untreated
TERS
Ern1 fl/fl
Ern1 x LysMCre

Fig 5.

A

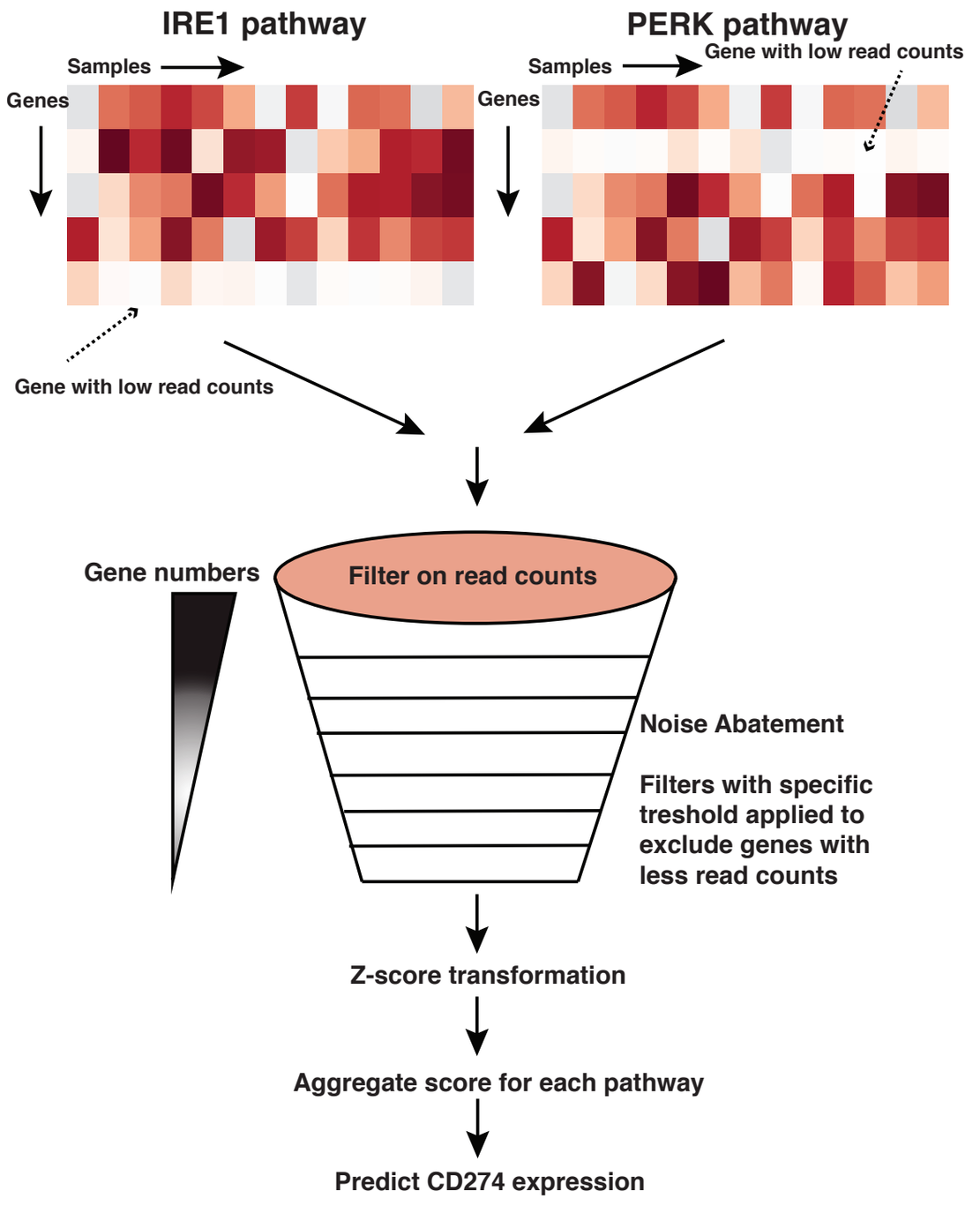
IRE1 pathway
PERK pathway
Samples
Genes
Gene with low read counts
Gene numbers
Filter on read counts
Noise Abatement
Filters with specific treshold applied to exclude genes with less read counts
Z-score transformation
Aggregate score for each pathway
Predict CD274 expression

B

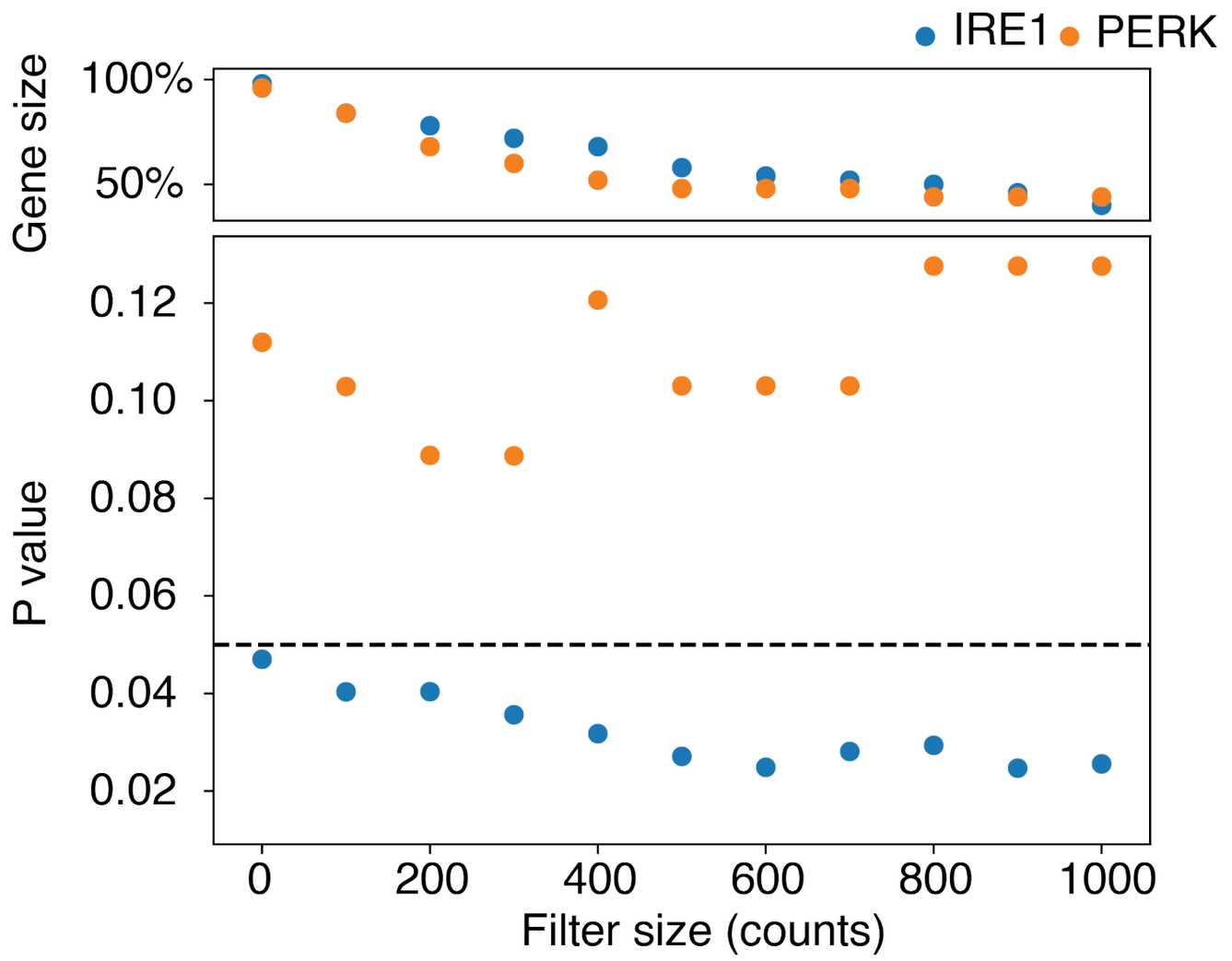
IRE1
PERK
Gene size
100%
50%
P value
0.12
0.10
0.08
0.06
0.04
0.02
0
200
400
600
800
1000
Filter size (counts)

Fig 6.

| | coef | pval |
|---|---|---|
| Intercept | 0.5681224413 | 0.6307185602 |
| BLCA | 3.730781629 | 0.00291005966 |
| BRCA | -0.281147938 | 0.8147005789 |
| CESC | 6.893379114 | 8.34E-08 |
| CHOL | 0.4014684074 | 0.8413656853 |
| COAD | 0.5300701923 | 0.6672164335 |
| DLBC | 20.84235676 | 8.08E-29 |
| ESCA | 3.017860087 | 0.03778129109 |
| GBM | -0.5684440601 | 0.6883179244 |
| HNSC | 5.61635157 | 5.51E-06 |
| KICH | 5.178474502 | 0.0023769321 |
| KIRC | -0.3455225035 | 0.7796198465 |
| KIRP | 0.6659839637 | 0.6060961809 |
| LGG | -0.639698116 | 0.6071139362 |
| LIHC | -0.2908561171 | 0.8160364346 |
| LUAD | 3.69555473 | 0.00272696993 |
| LUSC | 6.865457981 | 3.49E-08 |
| MESO | 1.141219118 | 0.4692291251 |
| OV | -0.1591619966 | 0.9007001625 |
| PAAD | -0.7801816419 | 0.5683066888 |
| PCPG | 2.243029289 | 0.09976162006 |
| PRAD | -0.1264243114 | 0.9190474856 |
| READ | 0.3292890692 | 0.8124095707 |
| SARC | -1.090528135 | 0.4092896389 |
| SKCM | 0.8616842823 | 0.5776724443 |
| STAD | 4.070734989 | 0.001469900349 |
| TGCT | 0.872136964 | 0.5455941353 |
| THCA | 2.317361301 | 0.06056962238 |
| THYM | 13.04353041 | 4.96E-19 |
| UCEC | -0.04793209811 | 0.9687882727 |
| UCS | -0.5462166032 | 0.7546040883 |
| UVM | 0.1250809139 | 0.9379339045 |
| ERN1.00 | -0.02639975541 | 0.3447808132 |
| gmeanMacro | 0.04256029965 | 1.93E-07 |
| ERN1:gmeanMacro | 0.001211494277 | 0.02397204832 |
| EIF2AK3 | -0.002925408763 | 0.8832796928 |
| EIF2AK3:gmeanMacro | 0.0007820854511 | 0.1550669885 |

Table 1.